An Analytical Solution to Transient Composite Domain Diffusion and its Potential Applications

by

Steven Zak Brookshaw

A thesis

presented to the University of Waterloo

in fulfillment of the

thesis requirement for the degree of

Masters of Applied Science

in

Chemical Engineering

Waterloo, Ontario, Canada, 2020

© Steven Zak Brookshaw 2020

Author's Declaration

I hereby declare that I am the sole author of this thesis. This is a true copy of the thesis, including any required final revisions as accepted by my examiners.

I understand that my thesis may be made electrically available to the public.

Abstract

The work developed here was initially made to provide a comprehensive model for the modified Loschmidt cell, but the project evolved to derive a more robust transient composite domain diffusion (TCDD) model. The original work created a symmetrical TCDD model in cartesian coordinates. But the project grew to create a TCDD model for: any geometry, symmetric / non-symmetric and for any homogenous exterior boundary condition. The expansion of the work allows for this TCDD model to apply to more applications. Since, many complex experiments resort to quasi-steady state models to perform their analysis, when a more accurate TCDD model would be better suited. For instance, the need for a more accurate model for the modified Loschmidt cell was shown in [1], where the quasi-steady state model currently used to extract the effective diffusion coefficient had errors potentially as high as 100%. Whereas, the model developed here does not employ any assumptions regarding their experiment, and thus would yield better results. The model developed utilized Vodicka's Orthogonality to resolve the inhomogeneous boundary conditions applied to the interior boundaries of the composite domain. The model was validated experimentally, by adapting a known radial diffusion experiment to become a composite domain diffusion experiment. The experiment, created by Kim [2], was adapted by performing it on an annulus disk and retrieving the effective diffusivity using the TCDD model and comparing those results to the solid disk's. From this experiment it was statistically shown that the two models retrieved the same values, thus validating the TCDD model. Also, this thesis analyzed which solver was best to conduct parameter estimation on the model, by creating artificial data of a modified Loschmidt cell and fitting the known effective diffusivity that produced the concentration profile. It was discovered that in simple geometries, derivative based solvers work best. However, as the modified Loschmidt cell reached 8 different domains of diffusion, a brute force tactic was considerably more accurate. Therefore, since this model developed is equipped to replace the erroneous quasi-steady state model of the modified Loschmidt cell, it should be employed to perform its parameter estimation.

Acknowledgements

I acknowledge: my parents, Dr. Gostick, Dr. Ioannidis, Dr. Pritzker and Dr. Penlidis for your contributions to putting an end to this MASc.

Dedication

To the 1 and ½ people who might read this… why?

Table of Contents

List of Figures

List of Tables

1. Introduction

Breakthrough developments in advanced materials require detailed characterization of their properties, and this in turn requires a mathematical model to interpret the data and quantify the unknown property of the material. Some properties require sophisticated experiments, and these must have a model counterpart that is sufficiently advanced, or else significant error will be introduced into the parameter estimation, undermining the validity of the experimental results. Analytical mechanistic models are preferred for several reasons, including the fact that the error associated with the parameter estimation is easily quantified and, and in most cases it is much lower than numerical methods. In this work a generalized analytical solution to transient composite domain diffusion (TCDD) was developed. The solution was derived for diffusion through discrete regions with different properties, which is directly applicable to mass transport through a series of porous media layers such as electrodes found in fuel cells, zinc-air batteries, and some types of redox flow batteries. The aim of this work was specifically targeted at analyzing the Loschmidt diffusion experiment, the literature reports of which have universally used a quasi-steady-state approximation to analyze the result. Quasi-steady state models can fit experimental data well [3], even though their parameter estimates can deviate by more than 100% [1] from true values. Therefore, extracting accurate parameter estimates from these experiments requires more than a model that fits the data well, but describes the mechanism of the experiment properly. Although TCDD models were used as far back as the 1950's [4] & [5], their ability to estimate parameters has not been investigated thoroughly, which is a gap addressed by this work.

1.1. Motivation

Most TCDD models in the literature were derived for one specific scenario thus lack generality, and furthermore they do not approach the problem as a tool for parameter estimation [1], [6] & [7]. In other words, all existing applications of the TCCD model are aimed at predicting fluxes and/or species profiles in domains with known transport parameters, rather than the inverse problem of fitting a transport parameter based on measured fluxes or profiles. This thesis aims to fill that gap by creating a general model that can be used to extract more accurate parameter estimates from state-of-the-art characterization techniques that would be better represented with a TCDD model. For example, the application considered in this work is the Modified Loschmidt cell which characterizes the effective diffusion through thin porous media [3]. The original application of the Loschmidt cell was to measure binary diffusion coefficients by monitoring the transient diffusion species A from its reservoir into a connected reservoir filled with species B [8]. The 'modified' version of this experiment places a porous specimen between the reservoirs, and hence the diffusion rate is reduced by the effective diffusivity of the porous separator. In its original form a quasi-steady state model is suitable since there is no composite domain. Once the porous specimen is introduced as a separator, however, a composite domain is created and the complexity of the TCDD model is necessary [1]. This project was specifically aimed at creating a TCDD model for the Modified Loschmidt cell, however the work presents a general model that can be applied to many situations. The TCDD model formulated can simulate an arbitrary number of distinct domains of diffusion, with any homogeneous exterior boundary conditions applied, and in any coordinate system. This resulting formulation has been implemented as a Python package to ensure the model created can be used as easily as possible.

In addition to the generalized solution and numerical implementation, this thesis additionally proves that the derived model is capable of performing parameter estimation, and this was validated experimentally. The development of this model should lessen the need for experimentalist to rely on numerical methods or quasi-steady state models to characterize materials and replace it with a more reliable analytical model. Therefore, the motivation behind this project was to develop a general TCDD model using Vodicka's Orthogonality to improve upon current characterization tools.

2. Background

The model developed could be applied to many different applications, but to narrow down the topic this work primarily discussed how it pertains to diffusion through thin porous media. More specifically, the solution was applied to model the modified Loschmidt cell, which is a commonly used experiment for measuring the diffusive properties of thin porous media in the through-plane direction. This chapter will first describe the role of diffusion in fuel cells, then provide a review of Fick's law in it various forms including application to porous materials, survey two experimental technique for measuring effective diffusion coefficients which are both used in this work, and finally introduce Vodicka's Orthogonality that will be used to solve the transient form of Fick's law applied to composite domains.

2.1. Diffusion in Polymer Electrolyte Membrane Fuel Cells

One area where the rate of diffusion through porous materials is critical are electrochemical devices, such as fuel cells. Polymer electrode membrane (PEM) hydrogen fuels operate on the following principles: hydrogen gas oxidizes at the anode to produce protons; while oxygen gas reacts with protons that are transported through the PEM to produce water.

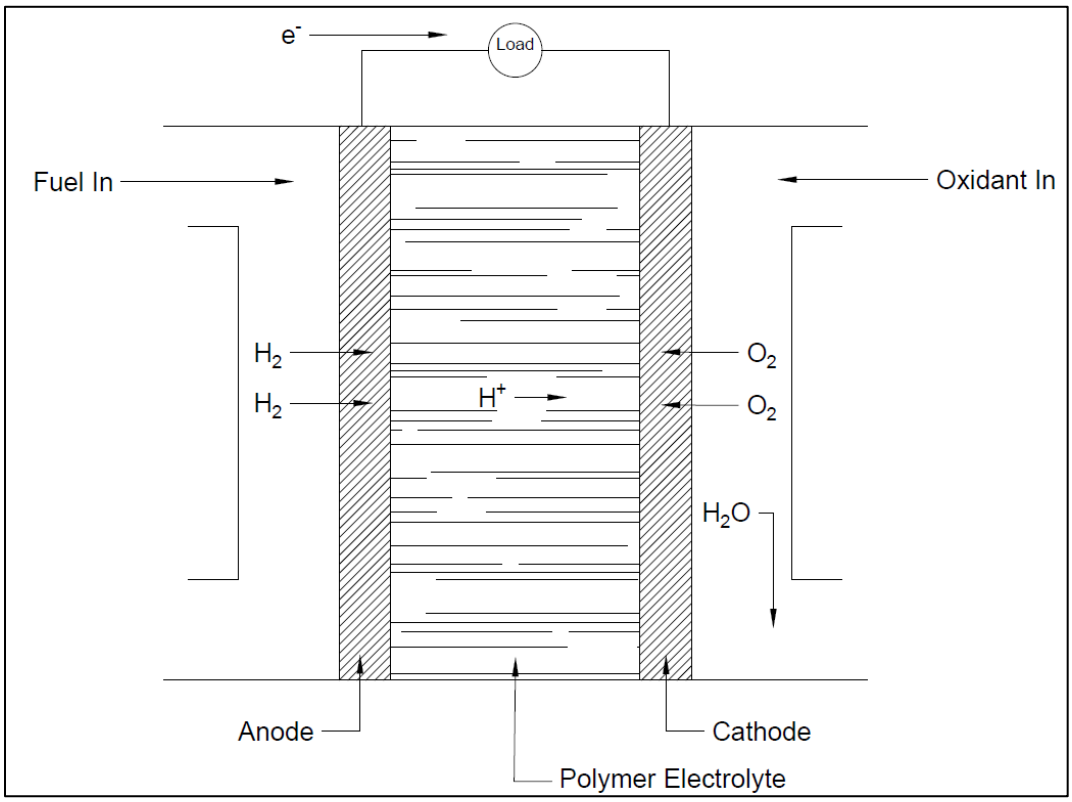

***Figure 1*:** Schematic of a PEM Hydrogen Fuel Cell

A PEM fuel cell's electrochemical process powers an external circuit, see Figure 1. Thin porous media and composite domain diffusion facilitate the transport of hydrogen/oxygen gas to the anode and cathode, respectively. A common electrode setup is to adhere a gas diffusion layer (GDL) to the catalyst layer connected by a microporous layer (MPL). The GDL serves several functions: distribute reactant more uniformly over the catalyst layer, drain produced water, structurally support the catalyst layer, transport current and dissipate heat [9]. Spreading the reactant, supplied by flow channels, to regions under the ribs is especially crucial to making a PEM commercially viable, since it aids in obtaining full utilization of the catalyst layer's expensive catalytic materials. The catalyst layer accounts for the largest cost of the PEM fuel cell, due to the rare/expensive materials required to catalyze the reactions, primarily platinum [9]. Figure 2, depicts an illustration of a typical PEM electrode.

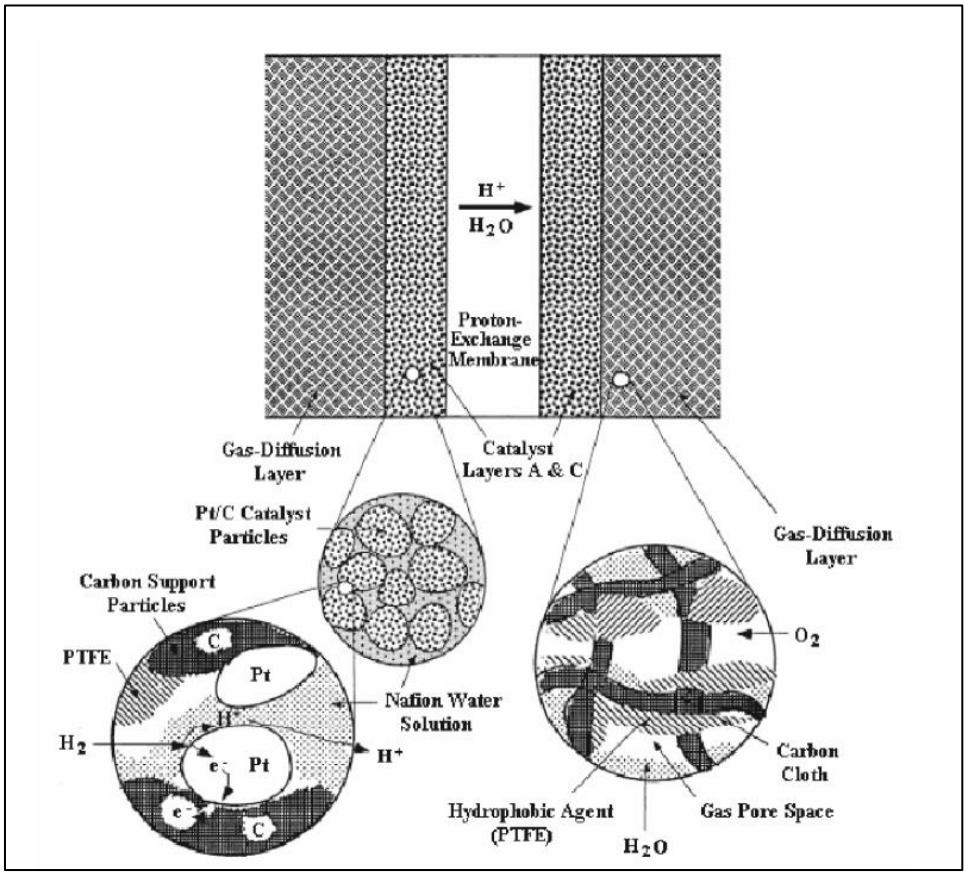

Figure 2: Diagram of a typical GDL / Catalyst Layer stack ***[9]***

Therefore, the feed gases (hydrogen and oxygen) must diffuse through multiple different layers of porous media in a PEM hydrogen fuel cell. The diffusion/mass transport of these species strongly dictates the

efficiency of the overall fuel cell. This necessitates a significant emphasis on the characterization of the effective diffusion coefficient of GDLs and catalyst layers in hydrogen fuel cell research. Mass transport will typically occur in two directions: through-plane and in-plane. The through-plane effective diffusion coefficient refers to the diffusion of reactant towards the catalyst, while the in-plane pertains to the lateral diffusion to the regions under the ribs, creating a more uniform concentration profile at the catalyst layer. In-plane measurements can be conducted with relative ease [2] [10] [11], but the through-plane direction presents a challenge due to the thinness of the materials. As such, the Loschmidt experiment is one of the only tools available.

2.2. Conservation of Mass in Porous Media

Describing mass transfer through a porous domain requires homogenizing the heterogenous domain. It assumes that the properties within the material are uniformly distributed; such that the solid phase's topographical effects are approximated using effective parameters which represents the hinderance the solid matrix exerts on mass transport in the pore space. Homogenization transforms the material into a continuum, and so conventional analytical modelling techniques can be applied to perform predictions or fit for the effective properties. Alternatively, to capture the true pore scale phenomena would necessitate 3D imaging and performing time consuming numerical methods on a voxel image of the porous media. Imaging in conjunction with numerical methods has several difficulties to overcome, such as: error propagation, image noise, time-consuming and expensive voxelated imaging. In many technical porous media (i.e. electrodes or vapor barriers), the property of interest is typically the effective diffusion coefficient. The effective diffusion coefficient is a measure of the porous media's ability to conduct gases through it via diffusion.

2.2.1. Fickian Diffusion

In 1855 Fick adopted the mathematics of heat conduction, first derived by Fourier in 1822, to the transport of mass driven by concentration gradients [12]. The mathematical theory of diffusion states that the diffusion flux of a material is proportional to the concentration gradient, in the normal direction to the area through which the material diffuses. Such that:

$$N_A = -D\,\nabla C_A \qquad \textbf{(1.)}$$

Therefore, incorporating Fick's first law into the conservation of mass in porous media (3.) results in:

$$\emptyset \frac{\partial C_A}{\partial t} = \; D\,\nabla^2 C_A \qquad \textbf{(2.)}$$

This governing equation dictates the behaviour of a Fickian diffusion mass transport process within a porous domain [13].

The treatment of mass conservation in homogenized porous media differs slightly from typical mass conservation in a true continuum since the presence of solid obstacles alters the volume available for accumulation. The underlying principle remains the same:

$$Accumulation = (Mass\ in) - (Mass\ out) + Generation$$

To illustrate consider a representative volume of some porous media with porosity "Ø" and a flux of species A across the boundary of the element, with no internal generation:

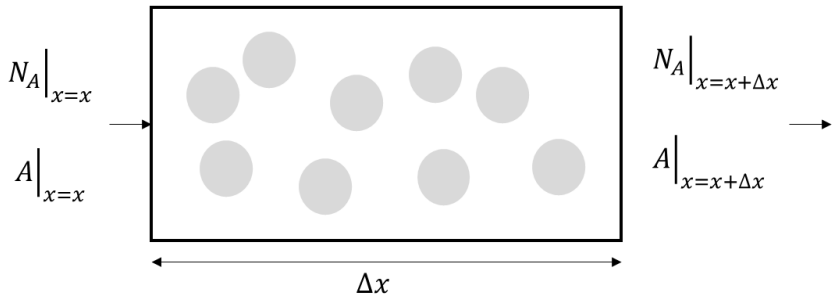

Figure 3: Diagram of Transient Flux through a porous volume element

Let C_A be the concentration of species A within the void space of the volume element and V be the total volume of the volume element. Therefore, the accumulation of mass within the void space is described as:

$$Accumulation = V\frac{\partial(C_A\emptyset)}{\partial t}$$

The definition of flux is needed to properly describe the $(Mass\ in/out)$ terms. The flux, N_A, is the molar rate of A to pass through a surface area. Therefore, the $(Mass\ in)$ and $(Mass\ out)$ terms are expressed as:

$$(Mass\ in) = N_A|_{x=x} \times A|_{x=x}$$

$$(Mass\ out) = N_A|_{x=x+\Delta x} \times A|_{x=x+\Delta x}$$

There are many modes of mass transport that can contribute to flux, but the one focused on is gradients in concentration, or Fickian diffusion.

The combination of these terms results in:

$$\emptyset\frac{\partial C_A}{\partial t} = -\nabla \cdot N_A \qquad \textbf{(3.)}$$

Therefore, the porosity of the porous media becomes an important factor in accounting for the reduced space that species A can occupy within porous media. Also note that the porous mass conservation equation reduces to its open space counterpart for a porosity of unity (open space).

2.2.2. Effective Properties in Porous Media

The standard binary diffusion coefficient in open air provides an upper limit of the effective diffusion coefficient, which is always lower since the porosity of the solid matrix reduces available area for flux, and the tortuous path around the matrix further inhibits mass transport. The tortuosity of the material is a measure of the extra distance that diffusing species must take through the pore space, defined as:

$$\tau = \left[\frac{Distance\ Travelled}{Displacement}\right]^2$$

The relationship between the effective diffusivity and the bulk 'open-air' value is given below. This equation also mathematically defines tortuosity which is essentially a fitting parameter to account for the fact that porosity alone does not explain the reduction of diffusivity observed in porous materials [13]:

$$D_{eff} = \frac{\emptyset}{\tau} D_{binary}$$

2.3. Experimental Characterization of Effective Diffusivity

2.3.1. Modified Loschmidt Cell

The original Loschmidt cell housed two separate gases in opposing and connected chambers or reservoirs. The experiment began by removing a solid plate that separated the two gases, allowing them to diffuse into one another. A probe located within one of the chambers measured the concentration of the invading gas, then the diffusion coefficient of the two gases would be calculated with the following equation which is an analytical solution to Fick's second law:

$$\boldsymbol{C}\,(\boldsymbol{x},\boldsymbol{t}) = \frac{\boldsymbol{C_{o,1}} + \boldsymbol{C_{o,2}}}{\boldsymbol{2}} + \left(\boldsymbol{C_{o,2}} - \boldsymbol{C_{o,1}}\right)\left(\frac{\boldsymbol{2}}{\boldsymbol{\pi}}\right)\sum_{\boldsymbol{m=0}}^{\infty} \frac{\boldsymbol{e}^{-\left(\frac{\boldsymbol{\pi}}{\boldsymbol{2L}}\right)^2 (\boldsymbol{2m+1})^2 \boldsymbol{D_{AB}} \boldsymbol{t}}}{\boldsymbol{2m+1}} \boldsymbol{sin}\left(\frac{\boldsymbol{\pi x}}{\boldsymbol{2L}}(\boldsymbol{2m+1})\right) \qquad (4.)$$

where L is the length of one of the two chambers; chamber 1 is located between $-L \leq x < 0$, and chamber 2 is $0 \leq x \leq L$; $C_{o,i}$ is the initial concentration of the "invading" species in chamber i; and D_{AB} is the diffusion coefficient of interest.

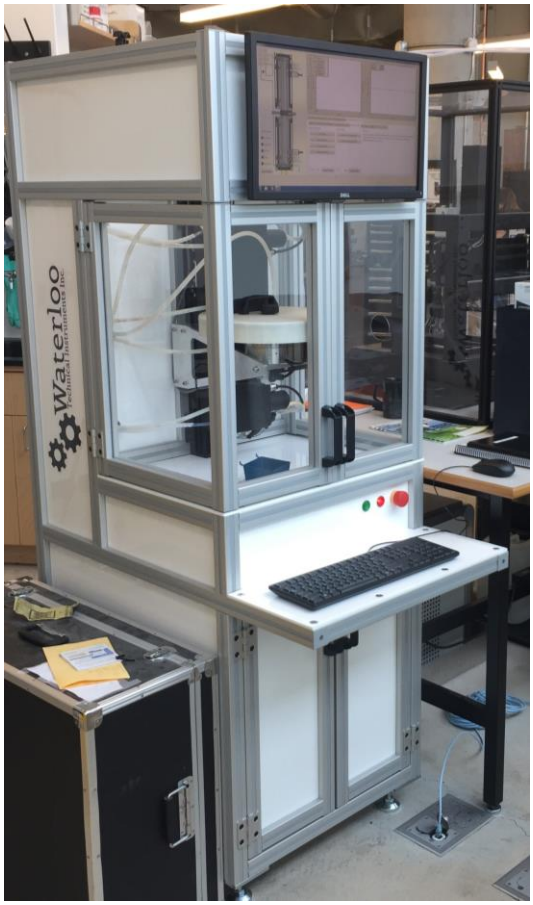

Figure 4: Photo of a modified Loschmidt cell, courtesy of Waterloo Technical Inc*. [3]*

The modified Loschmidt cell builds on the original design, by inserting thin porous media sample(s) at the center of the apparatus between the two chambers. Both chambers are still initially charged with different gases, typically oxygen and nitrogen since the diffusion coefficient of the species must be known in order to determine the effective diffusivity of the sample. The experiment proceeds in the same way, allowing the gases to diffuse into each other through the porous specimen, while a probe measures the oxygen concentration at one location. Thus, instead of binary diffusion, TCDD occurs [3] [1] [14], and from the concentration data collected the through-plane effective diffusion coefficients are estimated.

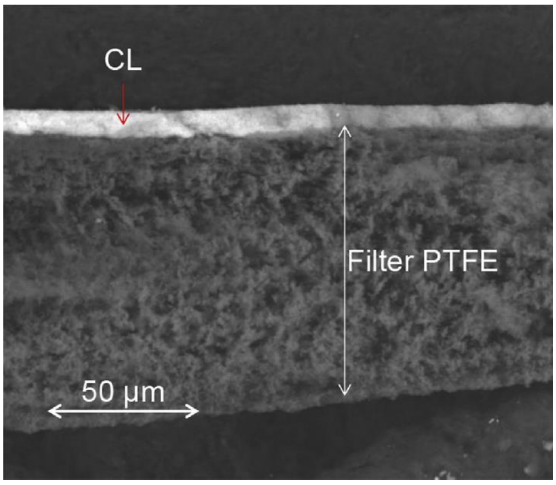

Figure 5: Example of a porous media "stack" studied with a modified Loschmidt cell ***[14]***.

Figure 4 shows a modified Loschmidt cell as built by Waterloo Technical Inc. In this setup "stacks" of porous media are analyzed, where multiple layers of porous media sample are layered upon one another. This is necessary for several reasons. Firstly, a single piece of thin porous media does not present a detectable reduction in mass flux, so several layers may be tested simultaneously to amplify the signal. Secondly, many porous materials are inherently multilayers, such as fibrous gas diffusion layers with a microporous coating on one side. Thirdly, some layers of interest are not self-supporting such as catalyst layers, so these must be applied to another layer for testing, such as a PTFE membrane. This is depicted in Figure 5. Lastly, due to the symmetry conditions used to obtain the analytical solution in (***4***.), it is necessary to create a symmetric stack of samples, so the layers of porous media are doubled as shown in Figure 6**.**

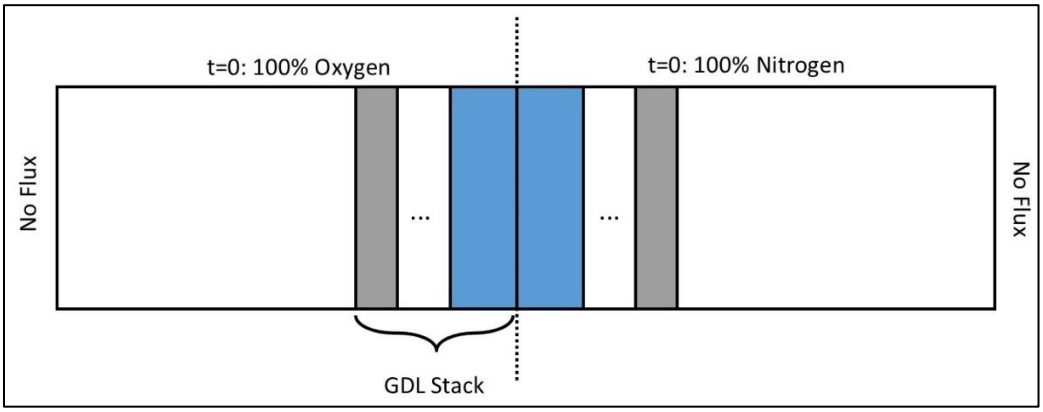

Figure 6: Diagram of symmetrical GDL (porous media) stacks

To conduct the experiment, the concentration of the invading gas, in this instance oxygen, is measured with a probe in the chamber that's initially saturated with nitrogen. The experiment can only determine a single effective diffusivity at a time; thus, to examine porous media stacks the experiment must be conducted iteratively, where each sample of porous media is isolated and analyzed individually [3] [14]. For example, the samples analyzed in [14] have two different types of porous media: a catalyst layer and PTFE filter. Before the catalyst layer with a PTFE filter could be analyzed, an experiment with just the PTFE filter alone was performed to fully characterize the PTFE and find its through-plane effective diffusion coefficient. Subsequently the experiment can be performed with the combined PTFE and catalyst layer, and the only unknown is the effective diffusivity of the catalyst layer. The concentration data collect in the modified Loschmidt cell is used to estimate the D_{AB} parameter in (***4***.), which becomes an equivalent diffusion coefficient that contains the diffusion in open space and the effective diffusivity of each layer in the stack. This equivalent coefficient must then be deconstructed to estimate the effective diffusion coefficient of a single porous media in the stack [3]. In all literature reports using the modified Loschmidt cell, a resistors in series approximation is used to relate the measured equivalent diffusion coefficient to the binary and effective diffusion coefficients, by the following relation;

$$R_{Total} = R_{binary} + \sum_{i=1}^{\#\ in\ stack} R_{stack,i}$$

where the resistances are related to diffusion coefficients by the following;

$$R_i = \frac{l_i}{D_i}$$

So, the iterative scheme of the experiment is as follows, first a single type of porous media is examined and is separated from the binary gas diffusion in open space as follows:

$$R_1 = R_{binary,1} + \sum_{i=1}^{n_1} R_{1,i}$$

Then, another experiment with the addition of one other porous media sample is conducted, and the new unknown effective diffusivity is found from:

$$R_2 = R_{binary,2} + \sum_{i=1}^{n_1} R_{1,i} + \sum_{i=1}^{n_2} R_{2,i}$$

It can be shown that the difference between these resistances results in the following expression;

$$R_2 - R_1 = R_{binary,2} - R_{binary,1} + \sum_{i=1}^{n_2} R_{2,i}$$

Applying Poulliet's law to these resistances yields:

$$\frac{L_{cell}}{D_{eq,2}} - \frac{L_{cell}}{D_{eq,1}} = \frac{L_{open,2} - L_{open,1}}{D_{binary}} + n_2 \frac{L_2}{D_{eff,2}}$$

where $D_{eff,2}$ is then isolated and solved for [3], [14].

This approach should be avoided for thin porous media, which was proven in [1].

2.3.2. Radial Diffusion Device

The Loschmidt device described above is used for measuring through-plane effective diffusivity. The in-plane direction is also of interest. One method developed by Kim and Gostick [2] uses a cylindrical geometry and allows diffusion through the radial periphery of the sample. The operating principles of this method are to suddenly change the boundary condition at the disk perimeter and measure transient concentration response via an oxygen probe located at the center of the porous media disk [2]. This data is then used to find the effective diffusion coefficient by fitting an analytical solution to Fick's section law in cylindrical coordinates [12]:

$$C(r,t) = C_o - (C_o - C_i)\frac{2}{R}\sum_{n=1}^{\infty} \frac{J_0(\lambda_n r)e^{-D\lambda_n^2 t}}{\lambda_n J_1(\lambda_n R)}$$

The eigenvalues (λ_n) are determined by:

$$J_0(\lambda_n R) = 0$$

The parameters and constants in the model are defined as: C_o is the boundary applied concentration, C_i is the initial concentration, D is the diffusivity of the domain and λ_n are the eigenvalues.

The above solution applies when the domain is at uniform initial concentration and a step change in the boundary conditions occurs at time 0. Experimentally these conditions are accomplished as follows: initially the porous media is saturated with air, then pure nitrogen gas was flowed vertically past the outer radius. The nitrogen gas was flowed orthogonally to the direction of diffusion, to avoid confounding any

convection effects into the experiment. Then the transient depletion of oxygen from the porous media into the flowing nitrogen stream is monitored by the oxygen probe. The transport of oxygen was purely diffusive; therefore, Fick's second law was applicable to model the mass transport, and so the effective diffusion coefficient can be fitted to the transient concertation data collected. Figure 7 contains a full schematic of the experimental device's design.

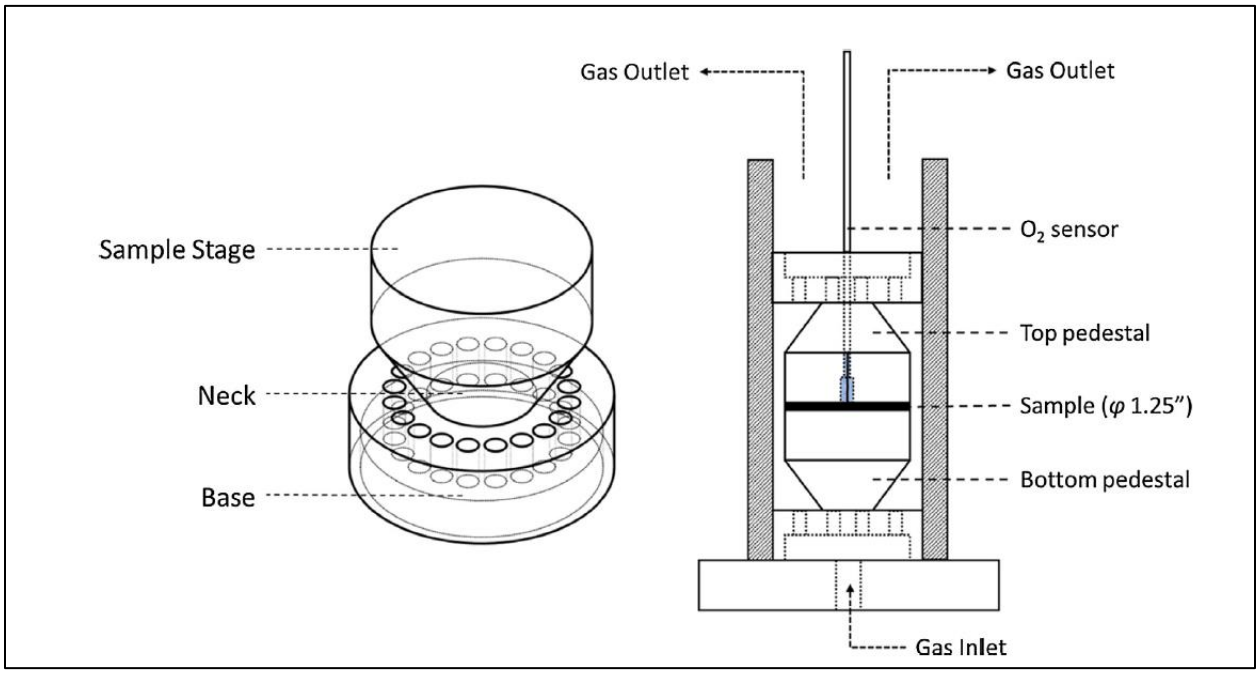

Figure 7: Schematic of Radial Diffusion Device ***[2]***

This device was used in the present work to validate the TCDD model. This experiment normally does not have a composite domain situation since materials are typically not layered, and non-self-supporting materials can also be tested. However, in this work composite domains were constructed by removing a disk from the middle and creating an annular shaped sample. This arrangement then has effective diffusion through the porous media, and open-space diffusion in the center disk. This is discussed in more detail in the Experimental Validation section.

2.4. Vodicka's Orthogonality

Conventional Strum-Liouville Orthogonality is not equipped to be applied to TCDD situations, since it cannot resolve the in-homogeneous interior boundary conditions that naturally arise. Though, in 1955,

Vodicka proved a form of Orthogonality that resolves the in-homogeneous boundary conditions of transient conduction through composite domains [5]. The in-homogenous boundary conditions are continuous flux and perfect or imperfect contact between boundaries [15]. Vodicka's Orthogonality is applied similarly to Strum-Liouville Orthogonality, where: each spatial function is multiplied by itself, but with a different index; then the function is integrated over the spatial function's boundaries. Vodicka furthered the orthogonality relationship by multiplying each integral by its domain's porosity (for mass transport) and finally summed each domain's integral expression to obtain the following expression:

$$\sum_{i=1}^{N} \emptyset_i \int_{\zeta_{i-1}}^{\zeta_i} \boldsymbol{X_{i,m}(x) X_{i,n}(x) dx} = \begin{cases} \boldsymbol{0} \, ; \boldsymbol{m \neq n} \\ \boldsymbol{N_m} \, ; \boldsymbol{m = n} \end{cases}$$

For the proof of Vodicka's Orthogonality in cartesian coordinates see Vodicka's Orthogonality Proof in the appendices.

Most models developed using Vodicka's Orthogonality have been for heat transport, however the mathematical form for mass and heat transport is identical in most scenarios. Therefore, the results found from these models can be transferred to mass transport, with few modifications.

Vodicka's orthogonality has been applied in several literature studies, surveyed here. Chiba [15] developed an analytical solution to one-dimensional transient heat conduction in a composite cartesian domain. The exterior boundary conditions were in-homogeneous functions of time, while the interior boundary conditions were continuous heat flux, with perfect and imperfect thermal contact. The initial conditions for each domain were arbitrary functions of space. The model was developed for an arbitrary number of domains.

The solution of the problem required the use of both Vodicka's Orthogonality and the shifting function method. The in-homogeneous interior boundary conditions were resolved using Vodicka's Orthogonality. However, the exterior boundary conditions are also in-homogeneous, which Vodicka's Orthogonality cannot resolve. Instead, the shifting function method is applied which resolves time dependent boundary conditions, after applying several simplifying assumptions.

Numerical simulations were performed to determine the limitations of the shifting function method, and it was found that the method was accurate for short times. In contrast, when the exterior boundary conditions are homogeneous, the numerical and analytical solutions were within the margin of numerical

error. Thus, the shifting function method was found to have noticeable limitations, whereas Vodicka's Orthogonality did not [15].

Singh et al. [7] developed a closed form analytical solution to transient heat conduction in a multilayered annulus in polar coordinates where the composite domain expands through the radial direction, and boundary conditions are applied in the angular direction. The resulting scenario had two spatial coordinates and two sets of eigenvalues.

Their solution is valid for homogeneous boundary conditions of the first and second kind applied to the angular exterior boundary, whereas the radial exterior boundary conditions are the first, second or third kind. Also, their solution accounts for internal generation that is a function of spatial coordinates but independent of time.

The closed form solution results in double series summation, as a result of the two sets of eigenvalues. Numerical simulations were performed to demonstrate that only a few terms need to be added in order to approach an acceptably low error threshold [7]. This is advantageous, since an explicit analytical solution is computationally less expensive and its upper bound of error is simply determined.

Monte [16] formulated a closed form solution to the transient heat conduction of two cartesian slabs in perfect contact, such that the heat flux and temperature along the interior boundary was continuous. The solution was developed for convective exterior boundary conditions. Monte solved for the eigenvalues by finding a transcendental equation formed by the boundary conditions. This is an alternative to the more common practice of solving for the roots of a boundary condition matrix's determinant, though both methods are equivalent. Since the closed form solution is an infinite series, the error associated with the series' truncation was observed and found that only 17 terms were required to reach an upper bound error of less than 1%.

Mikhailov et al [17], developed an algorithm to minimize the likelihood of omitting eigenvalues. It is not possible to guarantee that all eigenvalues are found from the transcendental equation that they belong to; and neglecting small eigenvalues will result in significant error in the truncated sum of the closed form analytical solution. Therefore, a convenient set of steps to reduce the odds of ignoring an important eigenvalue is incredibly important. The algorithm was formulated for transient heat conduction in cartesian, cylindrical and spherical coordinates, axial and radial coordinates. The boundary conditions applied for the derivation are convective heat flux along each exterior boundary; and continuous heat flux as well as continuous/discontinuous temperature at all interior boundaries.

Izadmehr et al [1], derived a composite domain model of Fick's second law, with boundary conditions that resemble the operating conditions of a modified Loschmidt cell containing a single porous media sample [1]. The purpose of their study was to develop a model that requires fewer simplifying assumptions and determine the error of the model currently in wide use by experimentalist. The model currently used assumes quasi-steady state conditions, which is an unnecessary simplification. The boundary conditions of a modified Loschmidt are no flux at either exterior boundary, and continuous mass flux and concentration along all interior boundaries. The initial conditions are such that one chamber is initially charged with oxygen, and the other would be pure nitrogen (or any gas other than oxygen), then the gases would be allowed to diffuse through the porous separator into one another. The analytical model was validated against numerical simulations, and the results proved the validity of the model's derivation.

The model was then used to perform an error analysis on the quasi-steady state model that's currently used to conduct the data analysis of the experiment. Their analysis concluded that the estimated effective diffusion coefficient would often produce erroneous estimates, especially if the experiment continues past 500 seconds. Therefore, it was recommended that the modified Loschmidt cell utilize a more mathematically rigorous model, otherwise the potential errors present in the effective diffusion coefficients would make all results untrustworthy [1].

The model's restricted to only account for one porous media sample, however current operations of the modified Loschmidt cell has at most 6 individual porous media samples at once [14]. Therefore, it is not capable of correcting all the errors of the previous experimental results.

3. Analytical Composite Domain Diffusion Derivation

3.1. Model Formulation

In the following subsections an analytical solution to TCDD is formulated. The set of PDEs and associated boundary conditions describes a species' diffusion through a series of porous media, for any geometry.

3.1.1. Governing Equation

TCDD obeys the fundamental mass transport equation within each domain, the difficulty primarily arises from the coupling of the interior boundary conditions. Therefore, the conventional mass transport equation was the starting point for this derivation [12]:

$$\emptyset_i \frac{\partial C_i}{\partial t} = D_i \nabla^2 C_i$$

For $i = 1 \dots N$, where N is the number of composite regions, C_i is the concentration of species i in the void space and D_i is the effective diffusion coefficient. However, to ease calculations the porosity $\emptyset_i$ and effective diffusion coefficient are combined to a single parameter:

$$D_i' = \frac{D_i}{\emptyset_i}$$

Therefore, the alternative form of the conventional mass transport equation becomes:

$$\frac{\partial C_i}{\partial t} = D_i' \nabla^2 C_i \qquad \textit{(5.)}$$

The effective diffusion coefficient is a combined term, with multiple parameters multiplied together. The correct definition of D_i would be $\frac{\emptyset_i D_{binary}}{\tau_i}$. In contrast, the combined effective diffusion coefficient (D'_i) is defined as $\frac{D_{binary}}{\tau_i}$ from which the tortuosity (τ) can be directly estimated [2], [18].

The interior boundary conditions assume perfect contact, such that the concentration and molar flux at the boundaries are continuous:

$$C_{i-1}|_{z=z_{i-1}} = C_i|_{z=z_{i-1}} \qquad \textit{(6.)}$$

$$-D_i \frac{\partial C_i}{\partial z}\Big|_{z=z_{i-1}} = -D_{i-1} \frac{\partial C_{i-1}}{\partial z}\Big|_{z=z_{i-1}} \qquad \textit{(7.)}$$

Replacing D_i for D_i' in Equation (7.):

$$\emptyset_i D_i' \frac{\partial C_i}{\partial z}\Big|_{z=z_{i-1}} = \emptyset_{i-1} D_{i-1}' \frac{\partial C_{i-1}}{\partial z}\Big|_{z=z_{i-1}} \qquad \textit{(8.)}$$

For $i = 2 \dots N$, and z_{i-1} is the boundary separating regions i and $i-1$.

In order to homogenize the boundary conditions, which allows Vodicka's Orthogonality to be applied and solution to be found, the general solution (C_i) must be split up into the transient ($y_i(t,z)$) and steady-state ($C_i^{SS}(z)$) concentration solutions:

$$\boldsymbol{C_i(t,z) = C_i^{ss}(z) + y_i(t,z)} \qquad \textbf{(9.)}$$

After substituting Equation (9.) into Equation (5.) the governing equation for the transient solution becomes:

$$\frac{\partial y_i}{\partial t} = D_i' \nabla^2 y_i \qquad \textbf{(10.)}$$

The PDEs for each domain are then made dimensionless using the following parameters: D_{min}, the minimum diffusivity for any of the composite domains; R, the length of the *entire* domain; and y_{ref}, a reference concentration, then multiply each PDE by:

$$\frac{R^2}{D'_{min}} \frac{1}{y_{ref}}$$

Resulting in the new set of dimensionless PDEs:

$$\frac{\partial \eta_i}{\partial \tau} = \varepsilon_i \nabla^2 \eta_i \qquad \textbf{(11.)}$$

The new parameters are:

$$\tau = \frac{D_{\min} t}{R^2}$$

$$\varepsilon_i = \frac{D_i'}{D'_{min}}$$

$$\eta_i = \frac{y_i}{y_{ref}}$$

Note that the Laplacian is with respect to a new spatial variable $\xi = z/R$.

3.1.2. Separation of Variables

The solution to the dimensionless set of PDEs given in Equation (11.) requires the application of separation of variables, which yields the time and spatial functions for each geometry [17], [15], [7]. To apply separation of variables, let:

$$\boldsymbol{\eta_i = F_i(\xi)G_i(\tau)} \qquad \textbf{(12.)}$$

Then substitute Equation (12.) into Equation (10.), to obtain the following relation:

$$\boldsymbol{F_i \frac{dG_i}{d\tau} = \varepsilon_i G_i \nabla^2 F_i} \qquad \textbf{(13.)}$$

Equation (13.) can be rearranged, to result in two separate ordinary differential equations:

$$\boldsymbol{\frac{1}{\varepsilon_i G_i}\frac{dG_i}{d\tau} = \frac{1}{F_i}\nabla^2 F_i = -\lambda_i^2} \qquad \textbf{(14.)}$$

where the eigenvalues λ_i^2 are specific to each region [15] [7].

The form of the time function is known to be the same for all geometries, which is:

$$\boldsymbol{G_i(\tau) = e^{-\varepsilon_i \lambda_i^2 \tau}} \qquad \textbf{(15.)}$$

After rearranging the ordinary differential equation pertaining to the spatial function ($F_i(\xi)$) in Equation (14.) it becomes;

$$\boldsymbol{\nabla^2 F_i + \lambda_i^2 F_i = 0} \qquad \textbf{(16.)}$$

For all geometries the solutions to Equation (16.) are shown in Table 1 [12].

Table 1: Depicts solution to spatial functions for each geometry

Coordinate	Spatial Function	Abbreviation
Cartesian	$F_i(\xi) = A_i \sin(\lambda_i \xi) + B_i \cos(\lambda_i \xi)$	$f_{L,i}(\xi) = \sin(\lambda_i \xi)\,; f_{R,i}(\xi) = \cos(\lambda_i \xi)$
Cylindrical	$F_i(\xi) = A_i \mathrm{J}_0(\lambda_i \xi) + B_i Y_0(\lambda_i \xi)$	$f_{L,i}(\xi) = \mathrm{J}_0(\lambda_i \xi)\,; f_{R,i}(\xi) = Y_0(\lambda_i \xi)$
Spherical	$F_i(\xi) = A_i \frac{\sin(\lambda_i \xi)}{\xi} + B_i \frac{\cos(\lambda_i \xi)}{\xi}$	$f_{L,i}(\xi) = \frac{\sin(\lambda_i \xi)}{\xi}; f_{R,i}(\xi) = \frac{\cos(\lambda_i \xi)}{\xi}$

Also shown in Table 1 is an abbreviation for each equation, that allows each geometry's spatial function to be described as:

$$\boldsymbol{F_i(\xi) = A_i f_{L,i}(\xi) + B_i f_{R,i}(\xi)} \qquad \textbf{(17.)}$$

3.1.3. Exterior Boundary Conditions

There are two exterior boundaries on the domain each can have three possible boundary conditions applied: (i) constant value, (ii) constant flux and (iii) convective transfer. Exterior boundary conditions are only applied to regions 1 and N, since those are the only that interact with the exterior. Splitting the general solution into transient and steady-state solutions homogenized the exterior boundary conditions for the transient solution, which is shown in Table 2 for each scenario.

Table 2: List of exterior boundary conditions, where $i = 1$ or N

Boundary Condition	General form	Transient form
Constant Value	$C_i(t, z = z_i) = C^*$	$\eta_i(\tau, \xi = \zeta_i) = 0$
Constant Flux	$\left.\frac{\partial C_i}{\partial z}\right\|_{z=z_i} = Flux^*$	$\left.\frac{\partial \eta_i}{\partial \xi}\right\|_{\xi=\zeta_i} = 0$
Convective Flux	$-D_i \left.\frac{\partial C_i}{\partial z}\right\|_{z=z_i} = h_i(C_i(t, z = z_i) - C^\infty)$	$\left.\frac{\partial \eta_i}{\partial \xi}\right\|_{\xi=\zeta_i} = -Biot_i \ \eta_i(\tau, \xi = \zeta_i)$

3.1.4. Interior Boundary Conditions

The interior boundaries are assumed to be in perfect contact, where the concentration and flux along the partition of the two materials is continuous such that:

$$\boldsymbol{C_i(t, z_{i-1}) = C_{i-1}(t, z_{i-1})}$$

It is possible to have imperfect contact or contact resistance [15], however this is not done in the present work since the focus was on diffusion in porous materials.

Once the general solution is separated into steady and transient solutions the boundary conditions take the following form, respectively:

$$\boldsymbol{C_i^{ss}(z_{i-1}) = C_{i-1}^{ss}(z_{i-1})}$$

$$\boldsymbol{\eta_i(\tau, \xi = \zeta_{i-1}) = \eta_{i-1}(\tau, \xi = \zeta_{i-1})} \qquad \textbf{(18.)}$$

The continuous molar flow boundary condition takes the form:

$$-\emptyset_i \boldsymbol{D'_i} \frac{\boldsymbol{\partial C_i}}{\boldsymbol{\partial z}}\bigg|_{z_{i-1}} = -\emptyset_{i-1} \boldsymbol{D'_{i-1}} \frac{\boldsymbol{\partial C_{i-1}}}{\boldsymbol{\partial z}}\bigg|_{z_{i-1}}$$

And for steady and transient solutions the boundary condition becomes:

$$-\emptyset_i \boldsymbol{D'_i} \frac{\boldsymbol{dC_i^{ss}}}{\boldsymbol{dz}}\bigg|_{z_{i-1}} = -\emptyset_{i-1} \boldsymbol{D'_{i-1}} \frac{\boldsymbol{dC_{i-1}^{ss}}}{\boldsymbol{dz}}\bigg|_{z_{i-1}}$$

$$-\emptyset_i \boldsymbol{\varepsilon_i} \frac{\boldsymbol{\partial \eta_i}}{\boldsymbol{\partial \xi}}\bigg|_{\xi=\zeta_{i-1}} = -\emptyset_{i-1} \boldsymbol{\varepsilon_{i-1}} \frac{\boldsymbol{\partial \eta_{i-1}}}{\boldsymbol{\partial \xi}}\bigg|_{\xi=\zeta_{i-1}} \qquad \textbf{(19.)}$$

3.1.5. Initial Conditions

Initial conditions can either be uniform or non-uniform within the material. In fact, many commonplace experiments rely solely on the driving force of initial concentration gradients [3]. The initial condition of the general solution will be referred to as the following:

$$\boldsymbol{C_i(t = 0, z) = C_i^o(z)}$$

within the domain $z_{i-1} \leq z \leq z_i$.

$$\boldsymbol{C_i^o(z) = C_i^{ss}(z) + y_i(t = 0, z)}$$

Therefore, the initial condition, over the domain of $\zeta_{i-1} \leq \xi \leq \zeta_i$, for the dimensionless transient solution becomes:

$$\boldsymbol{\eta_i(\tau = 0, \xi) = \frac{C_i^o(z) - C_i^{ss}(z)}{y_{ref}} = \eta_i^o(\xi)} \qquad \textbf{(20.)}$$

3.2. *Model Solution*

3.2.1. *Applying Exterior Boundary Conditions*

For each boundary condition found in Table 2, substitute the separated variables expression for η_i. The expression for the constant value boundary condition is found by replacing η_i with the combination of Equations (15.) and (17.) which simplifies to:

$$\boldsymbol{A_i f_{L,i}(\xi = \zeta_i) + B_i f_{R,i}(\xi = \zeta_i) = 0} \qquad \textbf{(21.)}$$

For the case of constant flux boundary conditions mentioned above, the boundary conditions are given as:

$$\boldsymbol{A_i \left.\frac{df_{L,i}}{d\xi}\right|_{\xi=\zeta_i} + B_i \left.\frac{df_{R,i}}{d\xi}\right|_{\xi=\zeta_i} = 0} \qquad \textbf{(22.)}$$

And, finally the convective flux boundary condition results in:

$$\boldsymbol{A_i \left(\left.\frac{df_{L,i}}{d\xi}\right|_{\xi=\zeta_i} + Biot_i\, f_{L,i}(\xi = \zeta_i) \right) + B_i \left(\left.\frac{df_{R,i}}{d\xi}\right|_{\xi=\zeta_i} + Biot_i\, f_{R,i}(\xi = \zeta_i) \right) = 0} \qquad \textbf{(23.)}$$

Region 1 was set to be the *basis* region, meaning the eigenvalues and constant pairs of region 1 are used to build the eigenvalues and constant pairs for the rest of the regions. Now let:

$$\boldsymbol{\vec{N} C_1 = \begin{bmatrix} A_1 \\ B_1 \end{bmatrix}} \qquad \textbf{(24.)}$$

The $\vec{N}$ vector is a combination of the "left" and "right" spatial functions, which varies for each geometry and exterior boundary condition applied to region 1.

3.2.2. *Applying Interior Boundary Conditions*

Continuous concentration boundary condition between domains are expressed as:

$$\boldsymbol{\eta_i(\tau, \xi = \zeta_{i-1}) = \eta_{i-1}(\tau, \xi = \zeta_{i-1})}$$

for $i = 2 \ldots N$. Substituting η_j with the combination of Equations (15.) and (17.) gives:

$$\boldsymbol{G_i(\tau)(A_i f_{L,i}(\xi=\zeta_{i-1})+B_i f_{R,i}(\xi=\zeta_{i-1}))} \quad \textbf{(25.)}$$
$$\boldsymbol{=G_{i-1}(\tau)(A_{i-1} f_{L,i-1}(\xi=\zeta_{i-1})+B_{i-1} f_{R,i-1}(\xi=\zeta_{i-1}))}$$

The only non-constants in Equation (25.) are $G_i(\tau)$ and $G_{i-1}(\tau)$. For the expression to hold for all time, the time functions must take the form [6];

$$\frac{\boldsymbol{G_i(\tau)}}{\boldsymbol{G_{i-1}(\tau)}}=\boldsymbol{1} \quad \textbf{(26.)}$$

Therefore, by substituting Equation (15.) into Equation (26.), the following relation between eigenvalues can be formulated:

$$\boldsymbol{\left(-\varepsilon_i\lambda_i^2+\varepsilon_{i-1}\lambda_{i-1}^2\right)\tau=0}$$

$$\boldsymbol{\lambda_i=\sqrt{\frac{\varepsilon_{i-1}\lambda_{i-1}^2}{\varepsilon_i}}}$$

It can be recursively shown that every eigenvalue can be written as an expression of the *basis* eigenvalue:

$$\boldsymbol{\lambda_i=\lambda_1\sqrt{\frac{\varepsilon_1}{\varepsilon_i}}} \quad \textbf{(27.)}$$

Now Equation (25.) can be simplified to:

$$\boldsymbol{A_i f_{L,i}(\xi=\zeta_{i-1})+B_i f_{R,i}(\xi=\zeta_{i-1})=A_{i-1} f_{L,i-1}(\xi=\zeta_{i-1})+B_{i-1} f_{R,i-1}(\xi=\zeta_{i-1})} \quad \textbf{(28.)}$$

Additionally, applying continuous molar flow boundary condition between each interior regions gives:

$$\boldsymbol{-\emptyset_i\varepsilon_i\left(A_i\frac{df_{L,i}}{d\xi}\Big|_{\xi=\zeta_{i-1}}+B_i\frac{df_{R,i}}{d\xi}\Big|_{\xi=\zeta_{i-1}}\right)} \quad \textbf{(29.)}$$
$$\boldsymbol{=-\emptyset_{i-1}\varepsilon_{i-1}\left(A_{i-1}\frac{df_{L,i-1}}{d\xi}\Big|_{\xi=\zeta_{i-1}}+B_i\frac{df_{R,i-1}}{d\xi}\Big|_{\xi=\zeta_{i-1}}\right)}$$

Combining both interior boundary conditions into matrix form yields:

$$\begin{bmatrix} \boldsymbol{f_{L,i}(\xi=\zeta_{i-1})} & \boldsymbol{f_{R,i}(\xi=\zeta_{i-1})} \\ \boldsymbol{\emptyset_i \varepsilon_i \left.\frac{df_{L,i}}{d\xi}\right|_{\xi=\zeta_{i-1}}} & \boldsymbol{\emptyset_i \varepsilon_i \left.\frac{df_{R,i}}{d\xi}\right|_{\xi=\zeta_{i-1}}} \end{bmatrix} \begin{bmatrix} \boldsymbol{A_i} \\ \boldsymbol{B_i} \end{bmatrix}$$

$$= \begin{bmatrix} \boldsymbol{f_{L,i-1}(\xi=\zeta_{i-1})} & \boldsymbol{f_{R,i-1}(\xi=\zeta_{i-1})} \\ \boldsymbol{\emptyset_{i-1} \varepsilon_{i-1} \left.\frac{df_{L,i-1}}{d\xi}\right|_{\xi=\zeta_{i-1}}} & \boldsymbol{\emptyset_{i-1} \varepsilon_{i-1} \left.\frac{df_{R,i-1}}{d\xi}\right|_{\xi=\zeta_{i-1}}} \end{bmatrix} \begin{bmatrix} \boldsymbol{A_{i-1}} \\ \boldsymbol{B_{i-1}} \end{bmatrix}$$

Define a new 2 x 2 matrix $M_{i,j}$ as:

$$\boldsymbol{M_{i,j}} = \begin{bmatrix} \boldsymbol{f_{L,i}(\xi=\zeta_j)} & \boldsymbol{f_{R,i}(\xi=\zeta_j)} \\ \boldsymbol{\emptyset_i \varepsilon_i \left.\frac{df_{L,i}}{d\xi}\right|_{\xi=\zeta_j}} & \boldsymbol{\emptyset_i \varepsilon_i \left.\frac{df_{R,i}}{d\xi}\right|_{\xi=\zeta_j}} \end{bmatrix} \quad \textbf{(30.)}$$

The interior boundary condition matrix thus becomes:

$$\boldsymbol{M_{i,i-1}} \begin{bmatrix} \boldsymbol{A_i} \\ \boldsymbol{B_i} \end{bmatrix} = \boldsymbol{M_{i-1,i-1}} \begin{bmatrix} \boldsymbol{A_{i-1}} \\ \boldsymbol{B_{i-1}} \end{bmatrix} \quad \textbf{(31.)}$$

3.2.3. Solving for Eigenvalues

The eigenvalues produced in Equation (14.) need to be found through the combination of Equations (21.), (22.), (23.) and (31.), to create a 2N by 2N coefficient matrix. Then the regional eigenvalues can be expressed in terms of the *basis eigenvalue*. Finally, the eigenvalues are found by forcing the determinant of coefficient matrix to zero. Eigenvalues that force the determinant of the coefficient matrix to zero in turn make the paired constants for each region linearly dependent; this allows for each region's paired constants to be expressed in terms of the *basis* constants.

For the exterior boundary conditions, let the three different types found in Equations (21.), (22.) and (23.) be described as:

$$[\boldsymbol{Ext_{L,i}(\lambda_i)} \quad \boldsymbol{Ext_{R,i}(\lambda_i)}] \begin{bmatrix} \boldsymbol{A_i} \\ \boldsymbol{B_i} \end{bmatrix} = \boldsymbol{0} \quad \textbf{(32.)}$$

where $i = 1 \; or \; N$. The coefficient matrix is constructed using Equations (31.) and (32.) to yield the following matrix, which is an 2N by 2N sparse array:

$$\begin{bmatrix} \boldsymbol{Ext_{L,1}(\lambda_1)} & \boldsymbol{Ext_{R,1}(\lambda_1)} & \mathbf{0}\ \mathbf{0} & \mathbf{0}\ \mathbf{0} & \cdots & \cdots & \mathbf{0}\ \mathbf{0} \\ \left[\boldsymbol{M_{1,1}}\right] & & -[\boldsymbol{M_{2,1}}] & \mathbf{0}\ \mathbf{0} & \cdots & \cdots & \vdots \\ \mathbf{0}\ \mathbf{0} & & [\boldsymbol{M_{2,2}}] & -[\boldsymbol{M_{3,2}}] & \mathbf{0}\ \mathbf{0} & \cdots & \vdots \\ \vdots & & \mathbf{0}\ \mathbf{0} & \mathbf{0}\ \mathbf{0} & \ddots & \mathbf{0}\ \mathbf{0} & \vdots \\ \vdots & & \vdots & \vdots & [\boldsymbol{M_{i-1,i-1}}] & -[\boldsymbol{M_{i,i-1}}] & \vdots \\ \vdots & & \vdots & \vdots & \mathbf{0}\ \mathbf{0} & \ddots & -[\boldsymbol{M_{N,N-1}}] \\ \mathbf{0}\ \mathbf{0} & & \mathbf{0}\ \mathbf{0} & \mathbf{0}\ \mathbf{0} & \mathbf{0}\ \mathbf{0} & \mathbf{0}\ \mathbf{0} & \boldsymbol{Ext_{L,N}(\lambda_N)} \quad \boldsymbol{Ext_{R,N}(\lambda_N)} \end{bmatrix} \begin{bmatrix} \boldsymbol{A_1} \\ \boldsymbol{B_1} \\ \boldsymbol{A_2} \\ \boldsymbol{B_2} \\ \vdots \\ \boldsymbol{A_{i-1}} \\ \boldsymbol{B_{i-1}} \\ \boldsymbol{A_i} \\ \boldsymbol{B_i} \\ \vdots \\ \boldsymbol{A_N} \\ \boldsymbol{B_N} \end{bmatrix} = \vec{\mathbf{0}}$$

In more concise notation, the above matrix operation can be expressed as;

$$\underline{\boldsymbol{M_{coef}}}(\boldsymbol{\lambda_1}, \boldsymbol{\lambda_2}, \dots, \boldsymbol{\lambda_N})\, \overrightarrow{\boldsymbol{AB}} = \vec{\mathbf{0}}$$

Now, the coefficient matrix can be expressed as a function of the *basis* eigenvalue using Equation (27.):

$$\underline{\boldsymbol{M_{coef}}}(\boldsymbol{\lambda_1})\, \overrightarrow{\boldsymbol{AB}} = \vec{\mathbf{0}} \qquad \textbf{\textit{(33.)}}$$

Finally, values of λ_1 must be found that satisfy [17], [15], [7]:

$$\boldsymbol{det}\left(\underline{\boldsymbol{M_{coef}}}(\boldsymbol{\lambda_1})\right) = \mathbf{0} \qquad \textbf{\textit{(34.)}}$$

There are an infinite number of eigenvalues that will satisfy Equation (34.); thus, the model becomes an infinite sum.

3.2.4. Vodicka's Orthogonality

Vodicka's orthogonality applied to the initial conditions was used to solve for C_n (see Equation (24.)), for a given $\lambda_{1,n}$. When implementing Vodicka's orthogonality, as with Strum-Louisville orthogonality, the aim is to use the orthogonality property to reduce the infinite sum of η_i to a single summand [4], [5]. From which a closed form expression for C_n can be found.

Firstly, substitute Equations (15.) and (17.) into (20.) in order to equate the initial conditions to their associated spatial and time functions;

$$\eta_i^o(\xi) = \sum_{n=1}^{\infty} \left(A_{i,n} f_{L,i}(\xi) + B_{i,n} f_{R,i}(\xi) \right) \quad \textit{(35.)}$$

To find a more concise notation, Equation (31.) was used to find a relationship between the *basis* constants to the rest of the constants. Begin with Equation (31.):

$$M_{i,i-1,n} \begin{bmatrix} A_{i,n} \\ B_{i,n} \end{bmatrix} = M_{i-1,i-1,n} \begin{bmatrix} A_{i-1,n} \\ B_{i-1,n} \end{bmatrix}$$

Observe the interior boundary conditions between regions 1 and 2, by setting $i = 2$:

$$M_{2,1,n} \begin{bmatrix} A_{2,n} \\ B_{2,n} \end{bmatrix} = M_{1,1,n} \begin{bmatrix} A_{1,n} \\ B_{1,n} \end{bmatrix}$$

Substitute Equation (24.) to replace the *basis* constants:

$$M_{2,1,n} \begin{bmatrix} A_{2,n} \\ B_{2,n} \end{bmatrix} = M_{1,1,n} \vec{N} C_n$$

Therefore, an expression for region 2's constants become:

$$\begin{bmatrix} A_{2,n} \\ B_{2,n} \end{bmatrix} = M_{2,1,n}^{-1} M_{1,1,n} \vec{N} C_n$$

For concise notation, the following matrix was defined to generate the constants for any arbitrary region in the TCDD problem:

$$Q_{i,n} = \begin{cases} \begin{bmatrix} 1 & 0 \\ 0 & 1 \end{bmatrix} ; i = 1 \\ M_{i,i-1,n}^{-1} M_{i-1,i-1,n} ; i > 1 \end{cases}$$

Using this $Q_{i,n}$ matrix a relationship between the *basis* constants and any other region's constants is determined, which was found to be:

$$\begin{bmatrix} A_{i,n} \\ B_{i,n} \end{bmatrix} = \prod_{j=1}^{i} Q_{j,n} \vec{N} C_n \quad \textit{(36.)}$$

Therefore, after substituting Equation (36.) into Equation (35.) the initial condition of the transient function can be expressed as:

$$\eta_i^o(\xi) = \sum_{n=1}^{\infty} [f_{L,i,n}(\xi) \quad f_{R,i,n}(\xi)\,] \prod_{j=1}^{i} Q_{j,n} \vec{N} C_n \qquad \textbf{(37.)}$$

For porous mass transport Vodicka's Orthogonality takes the form [4], [5]:

$$\sum_{i=1}^{N} \emptyset_i \int_{\zeta_{i-1}}^{\zeta_i} X_{i,m}(x) X_{i,n}(x) dx = \begin{cases} 0\,; m \neq n \\ N_m\,; m = n \end{cases}$$

To get the initial condition into the form required to apply Vodicka's Orthogonality, multiply the initial condition expression by:

$$\emptyset_i [f_{L,i,m}(\xi) \quad f_{R,i,m}(\xi)\,] \prod_{j=1}^{i} Q_{j,m} \vec{N} C_m$$

Then integrate each expression from it lower to upper spatial boundary, and sum all expressions together to obtain the following:

$$\sum_{i=1}^{N} \emptyset_i \int_{\zeta_{i-1}}^{\zeta_i} \eta_i^o(\xi) \left([f_{L,i,m}(\xi) \quad f_{R,i,m}(\xi)\,] \prod_{j=1}^{i} Q_{j,m} \vec{N} C_m \right) d\xi$$

$$= \sum_{i=1}^{N} \emptyset_i \int_{\zeta_{i-1}}^{\zeta_i} \sum_{n=1}^{\infty} \left([f_{L,i,n}(\xi) \quad f_{R,i,n}(\xi)\,] \prod_{j=1}^{i} Q_{j,n} \vec{N} C_n \right) \left([f_{L,i,m}(\xi) \quad f_{R,i,m}(\xi)\,] \prod_{j=1}^{i} Q_{j,m} \vec{N} C_m \right) d\xi$$

Utilizing orthogonality property, where if the index $n \neq m$ then summed integrals are zero, the infinite sum can be reduced to a single summand where $n = m$:

$$\sum_{i=1}^{N} \emptyset_i \int_{\zeta_{i-1}}^{\zeta_i} \eta_i^o(\xi) \left([f_{L,i,m}(\xi) \quad f_{R,i,m}(\xi)\,] \prod_{j=1}^{i} Q_{j,m} \vec{N} C_m \right) d\xi$$

$$= \sum_{i=1}^{N} \emptyset_i \int_{\zeta_{i-1}}^{\zeta_i} \left([f_{L,i,m}(\xi) \quad f_{R,i,m}(\xi)\,] \prod_{j=1}^{i} Q_{j,m} \vec{N} C_m \right)^2 d\xi$$

After rearrangement, C_m becomes:

$$C_m = \frac{\sum_{i=1}^{N} \emptyset_i \int_{\zeta_{i-1}}^{\zeta_i} \eta_i^o(\xi)\left([f_{L,i,m}(\xi) \quad f_{R,i,m}(\xi)\,] \prod_{j=1}^{i} Q_{j,m}\vec{N}\right)d\xi}{\sum_{i=1}^{N} \emptyset_i \int_{\zeta_{i-1}}^{\zeta_i} \left([f_{L,i,m}(\xi) \quad f_{R,i,m}(\xi)\,] \prod_{j=1}^{i} Q_{j,m}\vec{N}\right)^2 d\xi} \tag{38.}$$

Finally, a complete expression for TCDD is expressed as:

$$C(\tau,\xi) = C^{ss}(\xi) + \sum_{n=1}^{\infty} [f_{L,i,n}(\xi) \quad f_{R,i,n}(\xi)\,] \prod_{j=1}^{i} Q_{j,n}\vec{N}C_n e^{-\varepsilon_1 \lambda_1^2 \tau} \tag{39.}$$

4. Results and Discussion

4.1. Solver Analysis

Unlike previous studies, the present work aims to use this model for parameter estimation. Since eigenvalues are functions of the parameters, the gradient with respect to the parameters could be problematic. As shown in Equations (31.) and (32.), the coefficient matrix becomes a function of the fitting parameters, and as the number of composite domains increases, the gradient of the eigenvalues with respect to the fitting parameters will become more sporadic. To examine this closer, artificial data was generated using the TCDD model, and various methods of determining the effective diffusion coefficient were conducted. This approach allows for noise-free "data" to be examined for which the effective diffusion coefficients for all domains are known. The data generated in this section is a simulation of the modified Loschmidt cell, since it is a prevalent composite domain diffusion device, and is one of the target devices for which this model and its associated software were developed.

4.1.1. Derivative-Based vs Brute Force Solver Performance

The modified Loschmidt cell was simulated using the TCDD model formulated, the experimental setup simulated resembles the experiments conducted in [14]. The thickness and diffusivity of the GDL stack was randomly generated between the values of: $300 - 600\ \mu m$ and $0.2 - 0.8$ of binary diffusion. The GDL stack used had ranges from 1 to 3 GDLs, creating 4 to 8 composite domains of diffusion. The simulation performed the fitting on 300 randomly generated GDL stacks, 100 samples per GDL stack size.

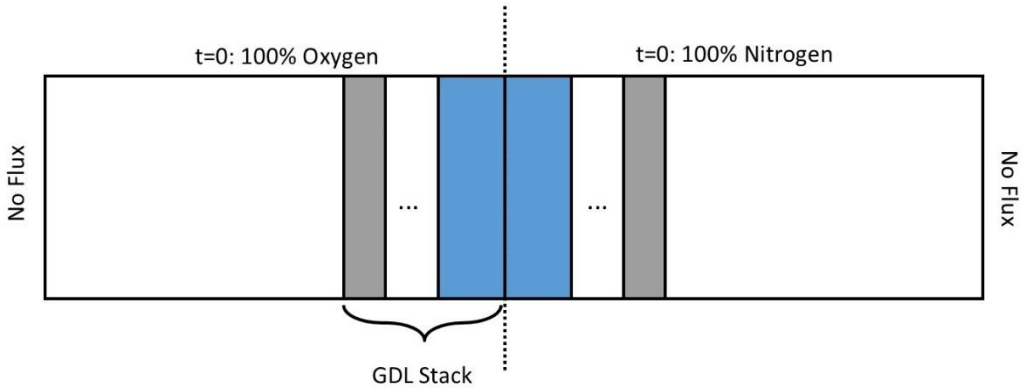

Figure 8: illustration of the simulated Modified Loschmidt Cell

The derivative-based solver used is known as "dogbox" which is implemented in the SciPy.optimization module. This is the recommended solver for minimizing least squares problems with rectangular constraints [19]. The brute-force technique assumes a unique minimum to the sum of square errors, and recursively restricts the domain over which it guesses parameters. The brute-force technique is taken as a baseline to compare the relative performance of the derivative based solver. Performance was measured by accuracy and time required to converge to a solution. The GDL whose diffusion coefficient is solved for is found on the interface between the GDL stack and open space (denoted by the grey zone in Figure 8) the remainder of the porous media's effective diffusivity is known. Also, the same artificially generated data is sent to both solvers.

Table 3: Solver's Average Performance

	dogbox		brute-force	
Domain Size	Time [sec]	Relative Error	Time [sec]	Relative Error
4	56.0	2.12E-11	138.7	7.33E-05
6	82.5	1.61E-11	195.4	2.58E-04
8	115.3	4.23E-03	251.3	1.68E-04

As can be seen in Table 3, the derivative solver was consistently much faster, therefore, the dog-box solver was adequately able to handle the sporadic derivatives with respect to the fitting parameter. Aside from a domain size of 8, the dog-box solver was more accurate than the brute-force technique, while taking approximately half the time. The runs with 8 domains of diffusion showed that the brute-force technique was $\approx 20 \times$ more accurate, which suggests that as the domain becomes more complex the derivative

solver's effectiveness is reduced. However, more than 8 domains of diffusion is a rare experimental condition, so the "dog-box" solver is generally recommended over the brute-force solver.

4.2. Experimental Validation

With the model having been shown to be capable of fitting artificially generated data with known diffusion coefficients, the next step was to show the model can be used for real experiments. Noise is present in all experiments, so for the TCDD model and its associated solver to effectively be implemented it must provide reasonable results despite the inevitability of instrumental noise. But more importantly, comparing the TCDD to a conventional and proven parameter estimation model will determine if the TCDD model works as intended.

4.2.1. Composite Radial Diffusion Experiments

In order to verify the model's ability to fit for diffusivities, the effective diffusivities of GDLs were measured according to the radial method of Yong and Gostick [2]. The experiment was run with solid disk GDLs, as well as with a ring disk. The solid disk is a single domain diffusion method, which has been proven to work as intended, and it used as a reference value to compare to the TCDD model. The ring disk creates a composite domain, since the outer disk is a porous GDL with the center being composed of open air. The effective diffusion coefficients of both samples were then found, and it was statistically determined if the effective diffusion coefficient values extracted from both methods are equivalent.

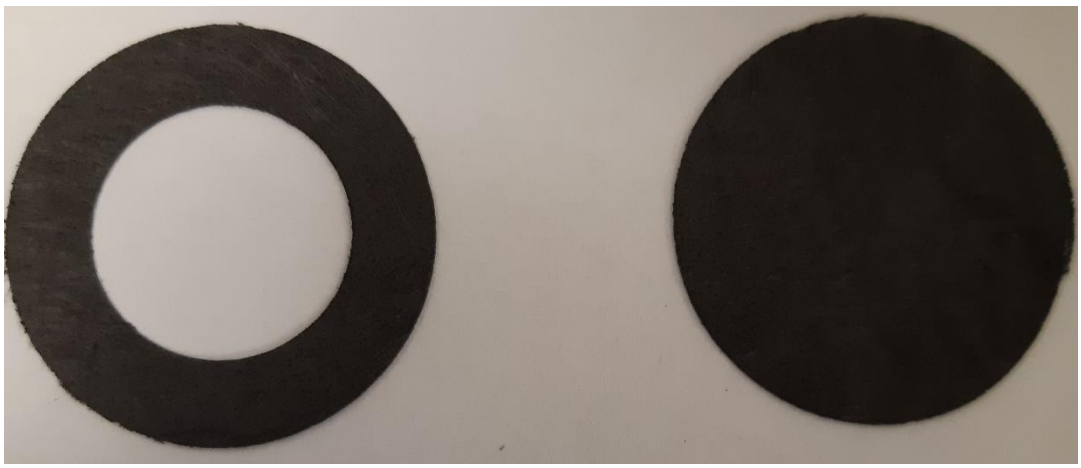

Figure 9: Image of the Composite Domain disk (left) and Solid disk (right)

Table 4 provides the diffusion coefficients determined for a variety of GDL materials, for both the composite domain tests on the ring disk (D^{comp}) and the full domain tests on the solid disk (D^{whole}).

Table 4: The fitting results for the composite and whole radial disk experiment

SGL-type	Porosity	D^{comp} $\left[\frac{m^2}{s}\right]$	D^{whole} $\left[\frac{m^2}{s}\right]$	$\frac{D^{comp}}{D_{binary}}$	$\frac{D^{whole}}{D_{binary}}$	Δd
24AA	0.884	1.46E-05	1.46E-05	7.23E-01	7.23E-01	0.00E+00
24AA		1.48E-05	1.49E-05	7.34E-01	7.36E-01	-2.09E-03
25AA	0.841	1.24E-05	1.24E-05	6.16E-01	6.14E-01	1.55E-03
25AA		1.21E-05	1.22E-05	5.99E-01	6.04E-01	-4.78E-03
34AA	0.854	1.30E-05	1.35E-05	6.42E-01	6.66E-01	-2.42E-02
34AA		1.36E-05	1.33E-05	6.75E-01	6.58E-01	1.66E-02
35BC	0.89	1.54E-05	1.47E-05	7.61E-01	7.29E-01	3.30E-02
35BC		1.51E-05	1.53E-05	7.46E-01	7.56E-01	-1.00E-02

The results are in near perfect agreement, but to be rigorous, a T-test was performed on the differences in the measurements (Δd) to determine if its mean is zero, which implies that there's no difference in the fitting done by the TCDD model and the traditional radial diffusion model. The alpha used for this two-tailed test was 5%, the calculations of the T-test found: $t_{obs} = 0.192$, and the $t_{\frac{0.05}{2},7} = 2.36$. Therefore, the null hypothesis was accepted and based on the data collected there is no observable difference between the fitted values of the TCDD model and the accepted radial diffusion model [2].

5. Concluding Remarks

5.1. Conclusions

An analytical solution to a TCDD model was formulated, with an arbitrary number of domains and for any conventional geometry. The solution was programmed into python, which was the software used to perform the data analysis in this thesis. The program provides an easy method to implement an analytical solution to characterizing relevant experiments and lessen the usage of potentially erroneous quasi-steady state models.

An analysis of whether the derivative based solver dogbox could be employed to this TCDD. The analysis was performed on randomly generated artificial concentration data of a modified Loschmidt cell. The

results of this found that for experiments with 6 or less domains the derivative solver was considerably faster and more accurate than the brute force solver. Though in the case of 8 domains of diffusion, the brute force solver was ~$20\times$ more accurate than the dogbox derivative solver tested.

The model was validated using a Radial diffusion device, where composite domain diffusion was created and compared to a known solution to its single domain counterpart. It was statistically proven that the effective diffusion coefficients found from the TCDD and single domain (ground truth) experiments were identical.

5.2. Recommendations

Upon the critiques found in [1] regarding the modified Loschmidt cell's quasi-steady state model, this experiment's characterization results would be more accurate with the use of a TCDD model. The model developed has been shown to be perfectly suited to meet this need. Specifically, since it has variable numbers of domains of diffusion and this model was developed to handle such scenarios.

It is suggested that any experiment that utilizes a quasi-steady state model to overcome the modelling difficulties of composite domain diffusion/conduction, should consider implementing this analytical solution. Since, the error associated with model inadequacy may be dramatically reduced

The techniques to solving the TCDD PDEs used in this work can also be applied to areas outside of mass transport through porous media. It is suggested that these other applications are explored.

6. References

[1] M. Izadmehr, M. Abbasi, M. Mansouri, A. Kazemi, A. Nakhaee and A. Daryasafar, "Accurate analytical model for determination of effective diffusion," *Fuel,* vol. 199, pp. 551-561, 2017.

[2] Y. Kim and J. Gostick, "Measuring effective diffusivity in porous media with a gasket-free, radial arrangement," *International Journal of Heat and Mass Transfer,* vol. 129, pp. 1023-1030, 2019.

[3] G. Unsworth, L. Dong and L. Xianguo, "Improved Experimental Method for Measuring Gas Diffusivity Through Thin Porous Media," *AIChE Journal,* vol. 59, no. 5, pp. 1409-1419, 2013.

[4] V. Vodicka, "Warmeleitung in geschichteten Kugel and Zylinderkörpern," *Schweizer Archiv,* vol. 10, pp. 297-304, 1950.

[5] V. Vodicka, "Eindimensionale Warmeleitung in geschichteten Körpern," *Mathematische Nachrichten,* pp. 47-55, 1955.

[6] F. d. Monte, "Transient heat conduction in one-dimensional composite slab. A `natural' analytic approach," *International Journal of Heat and Mass transfer,* vol. 36, pp. 3607-3619, 2000.

[7] S. Singh, P. Jain and Rizwan-uddin, "Analytical solution to transient heat conduction in polar coordinates with multiple layers in radial direction," *Internation Journal of Thermal Sciences,* vol. 47, pp. 261-273, 2008.

[8] J. Holman, Experimental Methods for Engineers, New York: Mcgraw Hill, 2012.

[9] J. Zhang, PEM Fuel Cell Electrocatalysts and Catalyst Layers, Vancouver: Springer, 2008.

[10] R. Rashapov and J. Gostick, "In-plane Effective Diffusivity in PEMFC Gas Diffusion Layers," *Transport in Porous Media,* vol. 115, pp. 411-433, 2016.

[11] T. Tranter, P. Stogornyuk, J. Gostick, A. Burns and W. Gale, "A method for measuring relative in-plane diffusivity of thin and partially saturated porous media: An application to fuel cell gas diffusion layers," *International Journal of Heat and Mass Transfer,* vol. 110, pp. 132-141, 2017.

[12] J. Crank, The Mathematics of Diffusion, Oxford: Clarendon Press, 1975.

[13] L. Shen and Z. Chen, "Critical review of the impact of tortuosity on diffusion," *Chemical Engineering Science,* vol. 62, no. 14, pp. 3748-3755, 2007.

[14] S. Salari, J. Stumper and M. Bahrami, "Direct measurement and modeling relative gas diffusivity of PEMFC catalyst layers: The effect of ionomer to carbon ratio, operating temperature, porosity, and pore size distribution," *International Jounral of Hydrogen Energy,* vol. 43, no. 34, pp. 16704-16718, 2018.

[15] R. Chiba, "An Analytical Solution for Transient Heat Conduction in a Composite Slab with Time-Dependent Heat Transfer Coefficient," *Hindawi,* pp. 1-11, 2018.

[16] F. d. Monte, "Transient heat conduction in one-dimensional composite," *International Journal of Heat and Mass Transfer,* pp. 3606-3619, 1999.

[17] M. D. MikHailov, M. N. Ozisik and N. L. Vulchanov, "Diffusion in Composite Layers with Automatic Solution of the Eigenvalue Problem," *International Journal Heat Mass Transfer,* vol. 26, no. 8, pp. 1131-1141, 1983.

[18] L. Shen and Z. Chen, "Critical review of the impact of tortuosity on diffusion," *Chemical Engineering Science,* vol. 62, no. 14, pp. 3748-3755, 2007`.

[19] "Sequential Quadratic Programming," in *Numerical Optimization*, New York, Spinger, 2006, pp. 529-531.

[20] G. Unsworth, "waterlooti," [Online]. Available: https://www.waterlooti.com/case-studies/the-loschmidt-cell. [Accessed 13 11 2019].

[21] J. Shen, J. Zhou, N. G. Astrath and e. al, "Measurement of effective gas diffusion coefficients of catalyst layers of PEM fuel cells with a Loschmidt diffusion cell," *Jounral of Power Sources,* vol. 196, pp. 674-678, 2011.

[22] D. Zanette and P. Alemany, "Thermodynamics of Anomalous Diffusion," *The American Physical Society,* vol. 75, no. 3, pp. 365-369, 1995.

[23] V. Balakrishnan, "Anomalous Diffusion in One Dimension," *Physica,* vol. 132, no. 2, pp. 569-580, 1985.

[24] A. Chaves, "A fractional diffusion equation to describe Levy flights," *Elsevier,* vol. 239, no. 1, pp. 13-16, 1998.

[25] J. Song and M. Bazant, "Electrochemical Impedance Imaging via the Distribution of Diffusion Times," *Physical Review Letters,* vol. 120, pp. 116001-116008, 2018.

[26] G. Padhy, C. Lemaire, E. Amirtharaj and M. Ioannidis, "Pore size distribution in multiscale porous media as revealed by DDIF-NMR, mercury porosimetry and statistical image analysis," *Colloids and Surfaces,* vol. 300, no. 1, pp. 222-234, 2007.

[27] M. Saccoccio, T. Wan, C. Chen and F. Ciucci, "Optimal Regularization in Distribution Relaxation Times applied to Electrochemical Impedance Spectroscopy: Ridge and Lasso Regression Methods - A Theoretical and Experimental Study," *Electrochimica Acta,* vol. 147, pp. 470-482, 2014.

[28] T. Jacobsen and K. West, "Diffusion Impedance in Planar, Cylindrical and Spherical Symmetry," *Electrochimica Acta,* vol. 40, no. 2, pp. 255-262, 1995.

[29] R. Rashapov, J. Unno and J. Gostick, "Characterization of PEMFC Gas Diffusion Layer Porosity," *Jounal of the Electrochemical Society,* vol. 162, no. 6, pp. 603-612, 2015.

7. APPENDICES

A. Vodicka's Orthogonality Proof

The following proof of Vodicka's Orthogonality is for Cartesian coordinates, or porous media mass transport with convective mass transport as the boundary conditions applied to both exterior boundary conditions. The convective mass transport boundary condition is used, since it is equivalent to constant value and constant flux boundary conditions under the following scenarios, if the mass transport coefficient is infinite then the boundary condition is a constant value, and if the mass transport coefficient is zero then the it is equal to a constant flux boundary condition. Now the proof is performed as follows:

$$\frac{d^2 F_{i,n}}{d\xi^2} + \lambda_{i,n}^2 F_{i,n} = 0 \qquad \textit{(40.)}$$

Using the following relation between each eigenvalue for each region found in [Eigenvalue Equ], relates each eigenvalue to the primary region (region 1):

$$\lambda_{i,n}^2 = \lambda_{1,n}^2 \frac{\alpha_1}{\alpha_i} \qquad \textit{(41.)}$$

The boundary conditions for each exterior surface are:

$$k_1 \left.\frac{dF_{1,n}}{d\xi}\right|_{\xi=\zeta_0} = h_1 \left. F_{1,n}\right|_{\xi=\zeta_0} \qquad \textit{(42.)}$$

$$k_N \left.\frac{dF_{N,n}}{d\xi}\right|_{\xi=\zeta_N} = h_N \left. F_{N,n}\right|_{\xi=\zeta_N} \qquad \textit{(43.)}$$

Notes that $k_i = \alpha_i \emptyset_i$, as per the derivation of the analytical model.

Each interior contact surface has the following two boundary conditions, first is continuous mass flux and the second is continuous concentration:

$$-\boldsymbol{k_i}\frac{\boldsymbol{dF_{i,n}}}{\boldsymbol{d\xi}}\Big|_{\xi=\zeta_{i-1}} = -\boldsymbol{k_{i-1}}\frac{\boldsymbol{dF_{i-1,n}}}{\boldsymbol{d\xi}}\Big|_{\xi=\zeta_{i-1}} \quad \textbf{(44.)}$$

$$\boldsymbol{F_i}|_{\xi=\zeta_{i-1}} = \boldsymbol{F_{i-1}}|_{\xi=\zeta_{i-1}} \quad \textbf{(45.)}$$

For $i = 2 \ldots N$

Insert (41.) into (40.) resulting in:

$$\frac{\boldsymbol{d^2F_{i,n}}}{\boldsymbol{d\xi^2}} + \boldsymbol{\lambda_{1,n}^2}\frac{\boldsymbol{\alpha_1}}{\boldsymbol{\alpha_i}}\boldsymbol{F_{i,n}} = \boldsymbol{0} \quad \textbf{(46.)}$$

Multiply (46.) by $F_{i,m}$ then integrate the equation from the start the end of its domain.

$$\int_{\zeta_{i-1}}^{\zeta_i}\left(\frac{\boldsymbol{d^2F_{i,n}}}{\boldsymbol{d\xi^2}} + \boldsymbol{\lambda_{1,n}^2}\frac{\boldsymbol{\alpha_1}}{\boldsymbol{\alpha_i}}\boldsymbol{F_{i,n}}\right)\boldsymbol{F_{i,m}}\boldsymbol{d\xi} = \boldsymbol{0} \quad \textbf{(47.)}$$

Perform integration by parts on the second derivative term in (47.):

$$\int_{\zeta_{i-1}}^{\zeta_i}\frac{\boldsymbol{d^2F_{i,n}}}{\boldsymbol{d\xi^2}}\boldsymbol{F_{i,m}}\boldsymbol{d\xi} = \frac{\boldsymbol{d\,F_{i,n}}}{\boldsymbol{d\xi}}\boldsymbol{F_{i,m}}\Big|_{\xi=\zeta_{i-1}}^{\xi=\zeta_i} - \int_{\zeta_{i-1}}^{\zeta_i}\frac{\boldsymbol{d\,F_{i,n}}}{\boldsymbol{d\xi}}\frac{\boldsymbol{dF_{i,m}}}{\boldsymbol{d\xi}}\ \boldsymbol{d\xi} \quad \textbf{(48.)}$$

Now substitute (48.) into (47.):

$$\frac{\boldsymbol{d\,F_{i,n}}}{\boldsymbol{d\xi}}\boldsymbol{F_{i,m}}\Big|_{\boldsymbol{\xi=\zeta_{i-1}}}^{\boldsymbol{\xi=\zeta_i}} - \int_{\boldsymbol{\zeta_{i-1}}}^{\boldsymbol{\zeta_i}} \frac{\boldsymbol{d\,F_{i,n}}}{\boldsymbol{d\xi}}\frac{\boldsymbol{dF_{i,m}}}{\boldsymbol{d\xi}}\ \boldsymbol{d\xi} + \boldsymbol{\lambda_{1,n}^2}\frac{\boldsymbol{\alpha_1}}{\boldsymbol{\alpha_i}}\int_{\boldsymbol{\zeta_{i-1}}}^{\boldsymbol{\zeta_i}} \boldsymbol{F_{i,n}F_{i,m}d\xi} = \boldsymbol{0} \qquad \textbf{(49.)}$$

Multiply (49.) by k_i then sum equation expression for $i = 1 \ldots N$

$$\sum_{\boldsymbol{i=1}}^{\boldsymbol{N}} \boldsymbol{k_i}\left(\frac{\boldsymbol{d\,F_{i,n}}}{\boldsymbol{d\xi}}\boldsymbol{F_{i,m}}\Big|_{\boldsymbol{\xi=\zeta_{i-1}}}^{\boldsymbol{\xi=\zeta_i}} - \int_{\boldsymbol{\zeta_{i-1}}}^{\boldsymbol{\zeta_i}} \frac{\boldsymbol{d\,F_{i,n}}}{\boldsymbol{d\xi}}\frac{\boldsymbol{dF_{i,m}}}{\boldsymbol{d\xi}}\ \boldsymbol{d\xi} + \boldsymbol{\lambda_{1,n}^2}\frac{\boldsymbol{\alpha_1}}{\boldsymbol{\alpha_i}}\int_{\boldsymbol{\zeta_{i-1}}}^{\boldsymbol{\zeta_i}} \boldsymbol{F_{i,n}F_{i,m}d\xi}\right) = \boldsymbol{0} \qquad \textbf{(50.)}$$

$$k_i \frac{d\,F_{i,n}}{d\xi}F_{i,m}\Big|_{\xi=\zeta_{i-1}}^{\xi=\zeta_i} = k_i \frac{d\,F_{i,n}}{d\xi}F_{i,m}\Big|_{\xi=\zeta_i} - k_i \frac{d\,F_{i,n}}{d\xi}F_{i,m}\Big|_{\xi=\zeta_{i-1}}$$

$$\begin{aligned}\sum_{i=1}^{N} k_i \frac{d\,F_{i,n}}{d\xi}F_{i,m}\Big|_{\xi=\zeta_i} - k_i \frac{d\,F_{i,n}}{d\xi}F_{i,m}\Big|_{\xi=\zeta_{i-1}} \\ = k_1 \frac{d\,F_{1,n}}{d\xi}F_{1,m}\Big|_{\xi=\zeta_1} - k_1 \frac{d\,F_{1,n}}{d\xi}F_{i,m}\Big|_{\xi=\zeta_0} + k_2 \frac{d\,F_{2,n}}{d\xi}F_{2,m}\Big|_{\xi=\zeta_2} - k_2 \frac{d\,F_{2,n}}{d\xi}F_{2,m}\Big|_{\xi=\zeta_1} \\ + \cdots + k_N \frac{d\,F_{N,n}}{d\xi}F_{N,m}\Big|_{\xi=\zeta_N} - k_N \frac{d\,F_{N,n}}{d\xi}F_{N,m}\Big|_{\xi=\zeta_{N-1}}\end{aligned}$$

Apply the interior boundary conditions in the following form:

$$-k_i \frac{dF_{i,n}}{d\xi}\Big|_{\xi=\zeta_{i-1}} F_i|_{\xi=\zeta_{i-1}} = -k_{i-1} \frac{dF_{i-1,n}}{d\xi}\Big|_{\xi=\zeta_{i-1}} F_{i-1}|_{\xi=\zeta_{i-1}}$$

Which eliminates all summands evaluated at an interior boundary condition, resulting in the sum to become:

$$\sum_{\boldsymbol{i=1}}^{\boldsymbol{N}} \boldsymbol{k_i}\frac{\boldsymbol{d\,F_{i,n}}}{\boldsymbol{d\xi}}\boldsymbol{F_{i,m}}\Big|_{\boldsymbol{\xi=\zeta_i}} - \boldsymbol{k_i}\frac{\boldsymbol{d\,F_{i,n}}}{\boldsymbol{d\xi}}\boldsymbol{F_{i,m}}\Big|_{\boldsymbol{\xi=\zeta_{i-1}}} = \boldsymbol{k_N}\frac{\boldsymbol{d\,F_{N,n}}}{\boldsymbol{d\xi}}\boldsymbol{F_{N,m}}\Big|_{\boldsymbol{\xi=\zeta_N}} - \boldsymbol{k_1}\frac{\boldsymbol{d\,F_{1,n}}}{\boldsymbol{d\xi}}\boldsymbol{F_{i,m}}\Big|_{\boldsymbol{\xi=\zeta_0}} \qquad \textbf{(51.)}$$

Substitute (51.) into (50.) for to obtain:

$$\sum_{\boldsymbol{i=1}}^{\boldsymbol{N}} \boldsymbol{\lambda_{1,n}^2}\frac{\boldsymbol{\alpha_1}}{\boldsymbol{\alpha_i}}\boldsymbol{k_i}\int_{\boldsymbol{\zeta_{i-1}}}^{\boldsymbol{\zeta_i}} \boldsymbol{F_{i,n}F_{i,m}d\xi} - \boldsymbol{k_i}\int_{\boldsymbol{\zeta_{i-1}}}^{\boldsymbol{\zeta_i}} \frac{\boldsymbol{d\,F_{i,n}}}{\boldsymbol{d\xi}}\frac{\boldsymbol{dF_{i,m}}}{\boldsymbol{d\xi}}\ \boldsymbol{d\xi} = \boldsymbol{0} \qquad \textbf{(52.)}$$

Now switch the n and m indexes in (52.)

$$\sum_{i=1}^{N} \boldsymbol{\lambda_{1,m}^2} \frac{\boldsymbol{\alpha_1}}{\boldsymbol{\alpha_i}} \boldsymbol{k_i} \int_{\zeta_{i-1}}^{\zeta_i} \boldsymbol{F_{i,n} F_{i,m} d\xi} - \boldsymbol{k_i} \int_{\zeta_{i-1}}^{\zeta_i} \frac{\boldsymbol{d\, F_{i,n}}}{\boldsymbol{d\xi}} \frac{\boldsymbol{dF_{i,m}}}{\boldsymbol{d\xi}} \; \boldsymbol{d\xi} = \mathbf{0} \qquad \textbf{(53.)}$$

Now perform (52.) − (53.)

$$\sum_{i=1}^{N} \lambda_{1,n}^2 \frac{\alpha_1}{\alpha_i} k_i \int_{\zeta_{i-1}}^{\zeta_i} F_{i,n} F_{i,m} d\xi - k_i \int_{\zeta_{i-1}}^{\zeta_i} \frac{d\, F_{i,n}}{d\xi} \frac{dF_{i,m}}{d\xi} \; d\xi$$
$$- \sum_{i=1}^{N} \lambda_{1,\mathrm{m}}^2 \frac{\alpha_1}{\alpha_i} k_i \int_{\zeta_{i-1}}^{\zeta_i} F_{i,n} F_{i,m} d\xi - k_i \int_{\zeta_{i-1}}^{\zeta_i} \frac{d\, F_{i,n}}{d\xi} \frac{dF_{i,m}}{d\xi} \; d\xi \; = 0$$

Which reduces to:

$$\left(\lambda_{1,n}^2 - \lambda_{1,\mathrm{m}}^2\right) \sum_{i=1}^{N} \frac{k_i}{\alpha_i} \int_{\zeta_{i-1}}^{\zeta_i} F_{i,n} F_{i,m} d\xi = 0$$

Recall the definition $k_i = \alpha_i \emptyset_i$:

$$\left(\lambda_{1,n}^2 - \lambda_{1,\mathrm{m}}^2\right) \sum_{i=1}^{N} \emptyset_i \int_{\zeta_{i-1}}^{\zeta_i} F_{i,n} F_{i,m} d\xi = 0$$

The expression above implies the following:

$$\sum_{i=1}^{N} \emptyset_i \int_{\zeta_{i-1}}^{\zeta_i} F_{i,n} F_{i,m} d\xi = \begin{cases} 0, if\ n \neq m \\ N_m, if\ n = m \end{cases}$$

Due to the following inequality:

$$\lambda_{1,n}^2 \neq \lambda_{1,\mathrm{m}}^2$$

Note, N_m is the solution to the following integral:

$$\sum_{i=1}^{N} \emptyset_i \int_{\zeta_{i-1}}^{\zeta_i} F_{i,m}^2 d\xi = N_m$$

Therefore, Vodicka's orthogonality has been proven for porous mass transport.

B. Experimental Data Fittings

The validation experimental data and curve fittings are presented in this section. The experimental results are for both the conventional use of the Radial Diffusion Device, which are denoted as solid cylinders in each figure caption. Also, the modified version meant to produce composite domain diffusion, which are referred to as disks in the figure captions. This experiment had the sole purpose of validating the TCDD model formulated in this work. Duplicate runs were performed, to increase the degrees of freed in the statistical analysis performed on this experiment, thusly there are runs 1 and 2 for each GDL type and geometry.

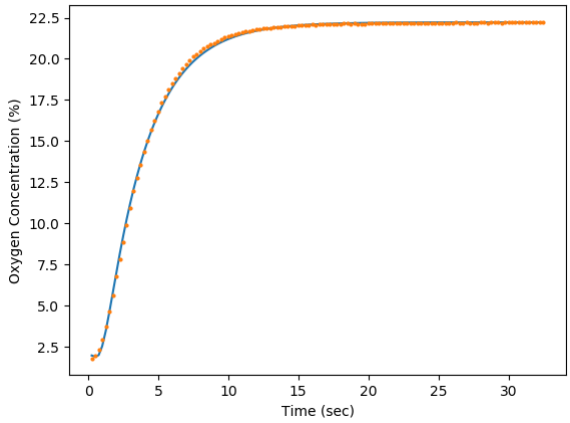

Figure 10: Concentration profile of SGL 24AA as a disk, run 1

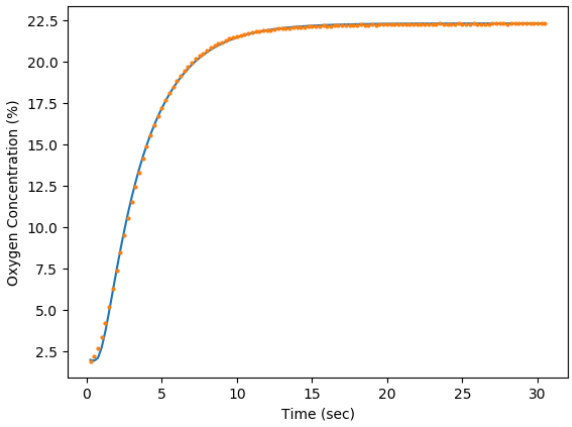

Figure 11: Concentration profile of SGL 24AA as a disk, run 2

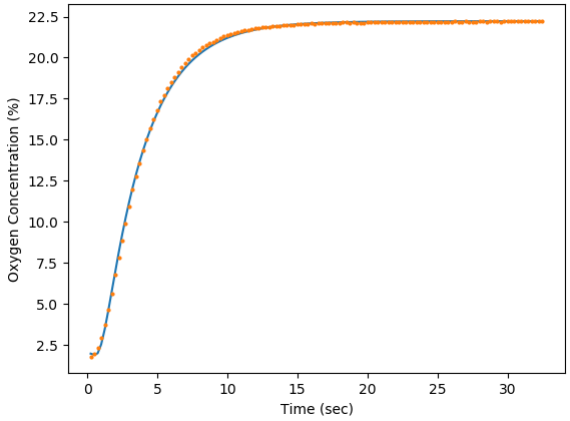

Figure 12: Concentration profile of SGL 24AA as a solid cylinder, run 1

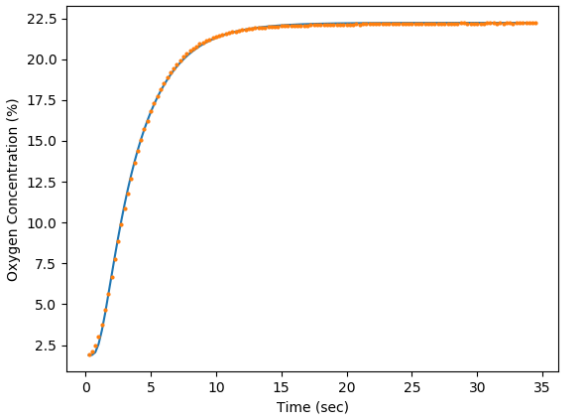

Figure 13: Concentration profile of SGL 24AA as a solid cylinder, run 2

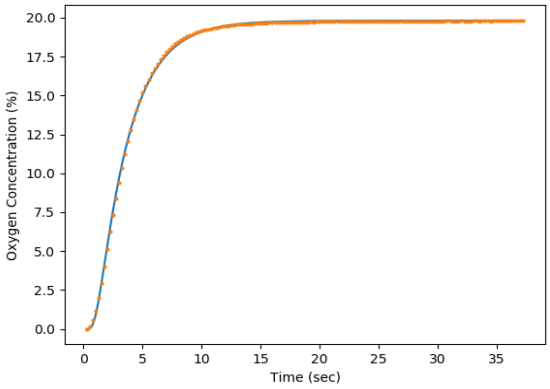

Figure 14: Concentration profile of SGL 25AA as a disk, run 1

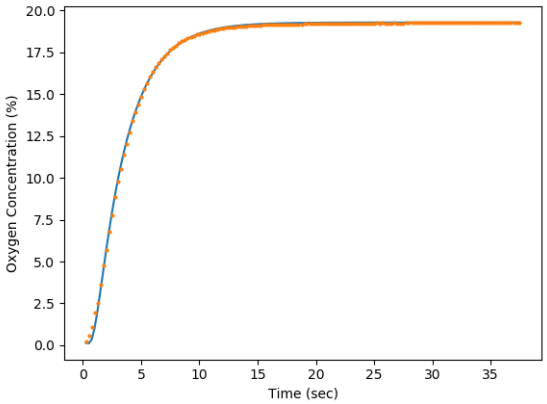

Figure 15: Concentration profile od SGL 25AA as a disk, run 2

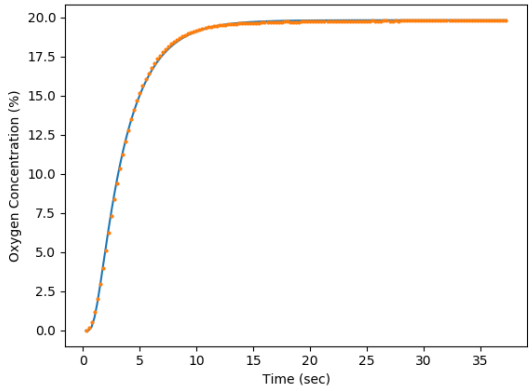

Figure 16: Concentration profile of SGL 25AA as a solid cylinder, run 1

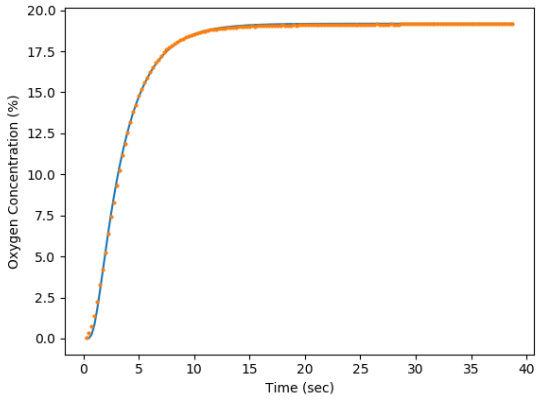

Figure 17: Concentration profile of SGL 25AA as a solid cylinder, run 2

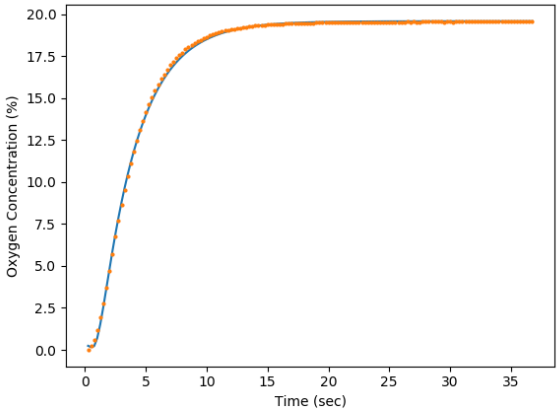

Figure 18: Concentration profile of SGL 34AA as a disk, run 1

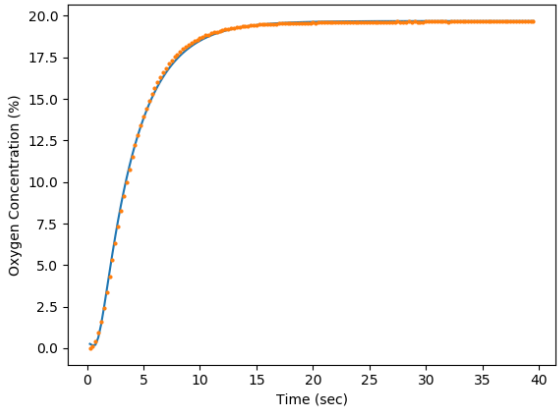

Figure 19: Concentration profile of SGL 34AA as a disk, run 2

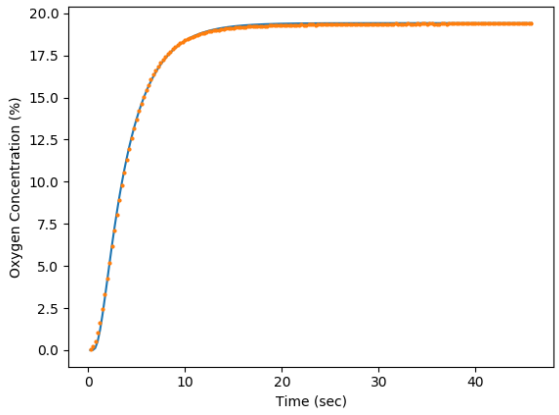

Figure 20: Concentration profile of SGL 34AA as a solid cylinder, run 1

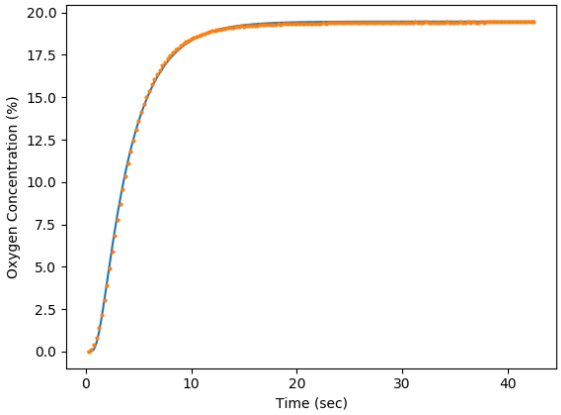

Figure 21: Concentration profile of SGL 34AA as a solid cylinder, run 2

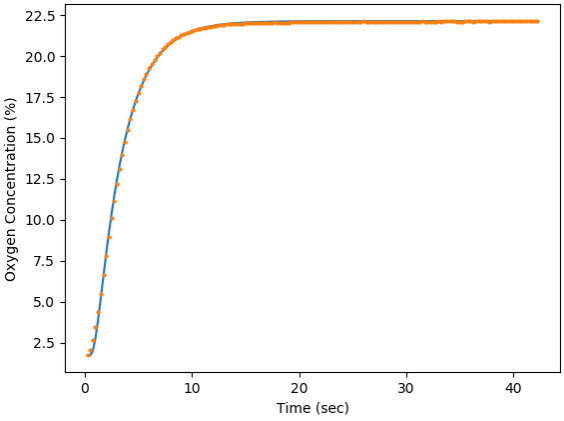

Figure 22: Concentration profile of SGL 35BA as a disk, run 1

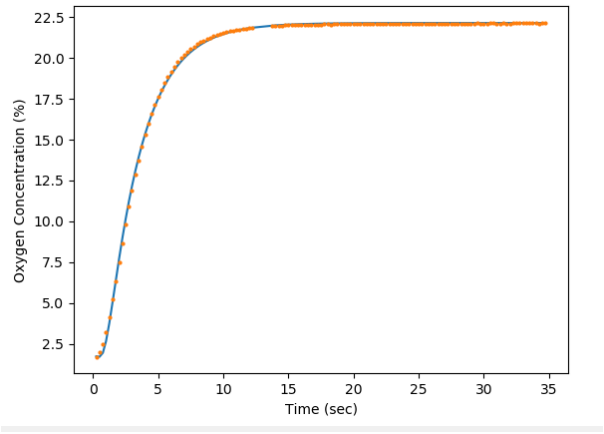

Figure 23: Concentration profile of SGL 35BA as a disk, run 2

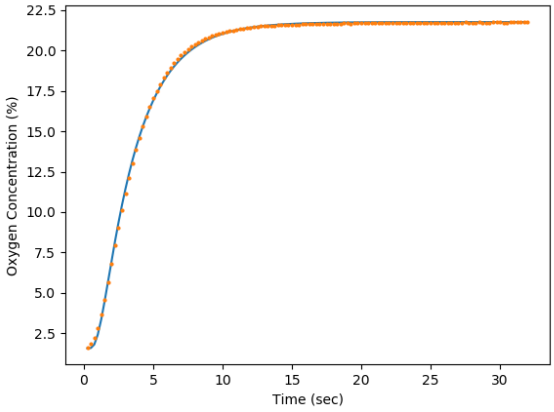

Figure 24: Concentration profile of SGL 35BA as a solid cylinder, run 1

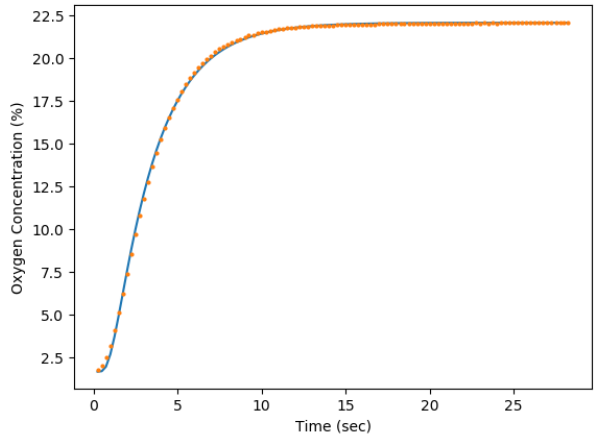

Figure 25: Concentration profile of 35BA as a solid cylinder, run 2